AD-A172 870 FURTHER STUDIES OF UNSTEADY TURBULENT BOUNDARY LAYERS 1/1
(U) IOWA INST OF HYDRAULIC RESEARCH IOWA CITY
B R RAMAPRIAN 25 SEP 86 ARO-19652 9-EG DAAG29-83-K-0004
UNCLASSIFIED F/G 20/4 NL

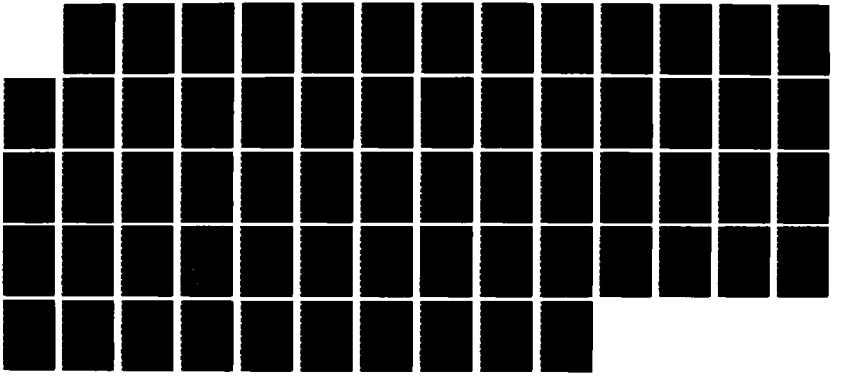

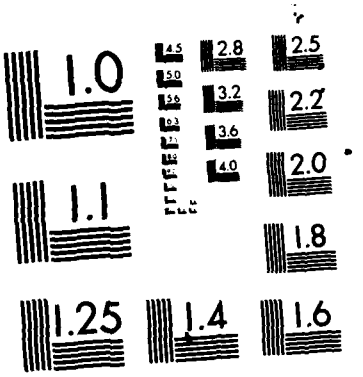

(2)

FURTHER STUDIES OF UNSTEADY TURBULENT BOUNDARY LAYERS

Final Technical Report

B.R. Ramaprian
Professor of Mechanical Engineering
Washington State University
Pullman, Washington

September 1986

The U.S. Army Research Office
Contract No. DAAG-29-83-K-004

UNIVERSITY OF IOWA
Institute of Hydraulic Research
Iowa City, Iowa 52242

MASTER COPY - FOR REPRODUCTION PURPOSES

UNCLASSIFIED
SECURITY CLASSIFICATION OF THIS PAGE (When Data Entered)

REPORT DOCUMENTATION PAGE		READ INSTRUCTIONS BEFORE COMPLETING FORM
1. REPORT NUMBER ARO 19652.9-EG	2. GOVT ACCESSION NO. N/A	3. RECIPIENT'S CATALOG NUMBER N/A AD-A172 870
4. TITLE (and Subtitle) Further Studies of Unsteady Turbulent Boundary Layers		5. TYPE OF REPORT & PERIOD COVERED Final Technical 10 Oct 82 - 30 Sep 86 6. PERFORMING ORG. REPORT NUMBER
7. AUTHOR(s) B.R. Ramaprian		8. CONTRACT OR GRANT NUMBER(s) DAAG29-83-K-0004
9. PERFORMING ORGANIZATION NAME AND ADDRESS Iowa Institute of Hydraulic Research University of Iowa Iowa City, IA 52242		10. PROGRAM ELEMENT, PROJECT, TASK AREA & WORK UNIT NUMBERS
11. CONTROLLING OFFICE NAME AND ADDRESS U. S. Army Research Office Post Office Box 12211 Research Triangle Park, NC 27709		12. REPORT DATE 25 September 1986 13. NUMBER OF PAGES
14. MONITORING AGENCY NAME & ADDRESS (if different from Controlling Office)		15. SECURITY CLASS. (of this report) Unclassified 15a. DECLASSIFICATION/DOWNGRADING SCHEDULE

16. DISTRIBUTION STATEMENT (of this Report)

Approved for public release; distribution unlimited.

17. DISTRIBUTION STATEMENT (of the abstract entered in Block 20, if different from Report)

NA

18. SUPPLEMENTARY NOTES

The view, opinions, and/or findings contained in this report are those of the author(s) and should not be construed as an official Department of the Army position, policy, or decision, unless so designated by other documentation.

19. KEY WORDS (Continue on reverse side if necessary and identify by block number)

Unsteady flows
Turbulent flows
Boundary layers
Periodic flows
Oscillatory boundary layers

20. ABSTRACT (Continue on reverse side if necessary and identify by block number)

Periodic turbulent boundary layers in zero and adverse time-mean pressure gradient have been studied. The study includes experimental, analytical and numerical investigations. The experiments were conducted in an unsteady-flow water tunnel, in which the freestream velocity varies sinusoidally with time around a mean value. Reduced frequencies up to about 25 and a relative oscillation amplitude of 40 per cent of the mean velocity were studied. Flow reversal occurred over a significant part of the oscillation cycle in the adverse pressure gradient experiments, though no mean-flow

DD FORM 1 JAN 73 1473 EDITION OF 1 NOV 65 IS OBSOLETE

UNCLASSIFIED
SECURITY CLASSIFICATION OF THIS PAGE (When Data Entered)

separation was observed. Data on turbulent stresses and wall shear stress were obtained using a two-component laser Doppler anemometry and a surface-mounted heat flux gage. A theory and calibration procedure were developed for the use of the latter in unsteady flow. All the experimental data have been recorded on magnetic tape. A general asymptotic theory has been developed for unsteady turbulent boundary layers. This theory leads to the development of wall functions for these flows. Such wall functions have been developed and used in a calculation procedure based on the k-ε model of turbulence.

A1

TABLE OF CONTENTS

Introduction 1
Experiments in Zero Pressure Gradient 2
An Asymptotic Theory for the Periodic TBL 7
Theory of the Use of Skin Friction Gage 12
Computational Studies 13
Experiments in Adverse Pressure Gradient 13
Concluding Remarks 17
References 18
Participating Scientific Personnel 20
Publications and Technical Reports 20
Tables 22
Figures 26

LIST OF TABLES

1. Similarity Laws for Periodic Turbulent Boundary Layers 22
2. Characterization of the Experiments for the Zero Pressure Gradient 23
3. Characterization of Other Experimental Studies 24
4. Mean-Flow Properties for the Adverse Pressure Gradient 25

LIST OF FIGURES

Fig.1. Lay-out of the water tunnel. 26
Fig.2. Longitudinal distribution of time-mean global properties of the boundary layer. 27
Fig.3. Mean velocity distributions in the boundary layer in the inner and outer coordinates. 28
Fig.4. Distribution of $\overline{u^2}$, $\overline{v^2}$, and $\overline{uv}$ at station 5. 29
Fig.5. Variation of $\langle C_f \rangle$ and $\langle u^2 \rangle$ during the oscillation cycle, station 5. 30
Fig.6. Behavior of the oscillatory component of $\langle U \rangle$ at station 5. 31
Fig.7. Behavior of the oscillatory component of $\langle u^2 \rangle$ and $\langle -uv \rangle$. 32
Fig.8. Frequency dependence of wall shear stress at station 5. 33
Fig.9. Oscillatory velocity components in the inner coordinates. 34
Fig.10. Oscillatory velocity components in the unsteady vortical layer coordinates. ..35
Fig.11. Qualitative representation of the evolution of the in-phase and out-of-phase velocity components with $\tilde{\omega}$. 36
Fig.12. oscillatory components of $\langle u^2 \rangle$, $\langle v^2 \rangle$ and $\langle -uv \rangle$ in unsteady vortical layer coordinates. 37
Fig.13. Correlation of the oscillatory wall shear stress in terms $\tilde{\omega}$. 38
Fig.14. Comparison of predictions with ZPG experimental data of amplitude and phase of velocity. 39
Fig.15. Comparison of predictions with ZPG experimental data of in-phase and out-of-phase components of Reynolds shear stress. 40
Fig.16. Imposed distribution of Clauser parameter β along the test section for the case of mild adverse pressure gradient. 41
Fig.17. Top wall geometries for mild and strong pressure gradients. 41
Fig.18. Details of the suction arrangement for the control of the boundary layer. 42
Fig.19. Longitudinal profiles of amplitude and phase of the freestream velocity. 43
Fig.20. Time-mean velocity distributions in mild adverse pressure gradient. 44
Fig.21. Long-time averaged Reynolds shear stresses in mild adverse pressure gradient. 45
Fig.22. Distributions of the amplitude of the oscillatory velocity in mild adverse

pressure gradient. 46
Fig.23. Variation of $\langle C_f \rangle$ during the oscillatory cycle in mild adverse pressure gradient. 47
Fig.24. Distributions of the phase of the oscillatory velocity in mild adverse pressure gradient. 48
Fig.25. Distributions of the amplitude of $\langle -uv \rangle$ in mild adverse pressure gradient. 49
Fig.26. Distributions of the phase of $\langle -uv \rangle$ in mild adverse pressure gradient. 50
Fig.27. Time-mean velocity distributions in strong adverse pressure gradient. 51
Fig.28. Long-time averaged Reynolds shear stresses in strong adverse pressure gradient. 52
Fig.29. Distributions of the amplitude of the oscillatory velocity in strong adverse pressure gradient. 53
Fig.30. Distributions of the phase of the oscillatory velocity in strong adverse pressure gradient. 54
Fig.31. Distributions of the amplitude of $\langle -uv \rangle$ in strong adverse pressure gradient. 55
Fig.32. Distributions of the phase of $\langle -uv \rangle$ in strong adverse pressure gradient. 56

INTRODUCTION

This project is a continuation of the earlier ARO Grant DAAG-29-79-G-0017. The overall objective of this project was to obtain additional experimental data on periodic turbulent boundary layers subjected to zero, as well as, adverse pressure gradients, from the unsteady-flow water tunnel constructed under the earlier ARO support. These experimental data would not only provide a comprehensive data base for use by the research community but also would directly be useful in the development of a theoretical framework for the description of unsteady turbulent boundary layers. The present contract work was started at the University of Iowa (UI) on October 1, 1982. While the work was in progress, the PI, Dr. B.R. Ramaprian resigned his position at the UI to take up the position of Professor of Mechanical Engineering at Washington State University (WSU) with effect from August 16, 1985. With the approval from ARO, the research work was continued by him at WSU, under a subcontract from UI to WSU, with Professor F. Stern of the Department of Mechanical Engineering at UI acting as a co-principal Investigator and being responsible for reporting to ARO. The experiments were completed at Iowa and the unfinished data processing and analysis were completed at WSU.

Problems Studied

The following tasks were performed under this contract.

1. Experiments on periodic turbulent boundary layers in time-mean zero pressure gradient.
2. Theoretical Analysis of unsteady turbulent boundary layers.
3. Computational studies on unsteady turbulent boundary layers.
4. Theoretical analysis of the performance of a surface-mounted heat-flux gage as a skin-friction gage in unsteady flow.
5. Experiments on periodic turbulent boundary layers in time-mean adverse pressure gradient.

The work performed and the important results obtained are summarized in the following sections. More details can be found from other sources such as thesis, journal articles, interim reports, etc. cited in this report.

EXPERIMENTS IN ZERO PRESSURE GRADIENT

These experiments were performed on a turbulent boundary layer which was subjected to a freestream-velocity variation of the form

$$U_e(t) = U_0(1 + \epsilon \sin \omega t) \tag{1}$$

with the time mean velocity U_0 and the relative amplitude of oscillation ϵ being both constant.

Apparatus and Instrumentation

The unsteady-flow water tunnel built under the earlier ARO support was used for these experiments. Figure 1 shows the layout of the tunnel. It works under a constant head of 8 m. The test section is 2.4 m long, with a rectangular cross-section 50 cm in width and 22.5 cm in height. Its bottom wall used as the test surface is a smooth brass plate. Transition was promoted by means of a strip of 14-mesh brass screen (15 cm wide) glued to the test surface at a distance of about 22.5 cm from the end of the contraction. The side walls of the tunnel are 9.5 cm thick steel plates, with 5 windows whose centerlines are located at approximately, x=48, 69, 90, 142, and 203 cm. These locations are designated as stations 1,2,3,4 and 5 respectively. The top wall of the test section is a Plexiglas sheet 37.5 mm thick. In addition, a 6.4 mm thick flexible Plexiglas sheet was used as a 'false' wall. By adjusting its position to correct for the displacement thickness of the boundary layer along the walls, a nearly zero (time-mean) longitudinal pressure gradient was obtained in the test section. The tunnel ends in a steel cylinder (40 cm diameter x 60 cm long) whose downstream end is closed. The cylinder has two longitudinal rectangular slots, 30 cm x 2.54 cm, located 180 degrees apart, from which the water exits. The area of opening of the slots is varied by a rotating profiled sleeve driven by a 3 H.P. geared D.C. motor whose speed can be regulated to within 1/4 %. Each complete rotation of the sleeve corresponds to two oscillation cycles. The sleeve profile is contoured to produce a sinusoidally varying velocity in the test section at the desired frequency. The details of design of the sleeve are given in Ramaprian and Tu (1982).

A frequency-shifted, tracker based, two-component Laser Doppler Anemometer (LDA) was used to measure the instantaneous longitudinal and normal velocity components in the boundary layer of the test surface. A surface-mounted TSI heat-flux gage (HFG) operated by a DISA constant-temperature anemometer was used for the measurement of wall shear stress. A theory for the use of this probe in unsteady flow is described in section 4. Measurement of wall shear stress was made at four stations: x=48 cm, 80 cm, 142 cm and 203 cm.

A HP/1000 minicomputer was used for data acquisition and processing. Signals from the LDA and HFG were sampled at 100 fixed phase positions in the oscillating

cycle. The instantaneous data obtained were processed using the well known "triple decomposition" principle (see for eg., Hussain and Reynolds 1970). This means that any instantaneous property Φ ($\Phi = U, V$ or τ_w) is expressed as

$$\Phi = \overline{\Phi}(x,y) + \Phi_p(x,y,\theta_p) + \phi(x,y,t) \tag{2}$$

where $\overline{\Phi}$ is the time-mean value, Φ_p the periodic deterministic component, ϕ the turbulent fluctuation and θ_p the phase position within a cycle. The first step, in practice, is to obtain the ensemble-averaged value $\langle\Phi\rangle(x,y,\theta_p)$ by averaging the instantaneous values at identical θ_p positions over a large number of oscillation cycles. The time-mean value $\overline{\Phi}$ is then obtained by averaging $\langle\Phi\rangle$ over the complete cycle ($0 < \theta_p < 2\pi$). The periodic component Φ_p is the difference $\langle\Phi\rangle - \overline{\Phi}$. Finally, the turbulent fluctuation ϕ is simply $\Phi - \langle\Phi\rangle$. This is a statistical quantity, for which the phase-averaged and time-averaged mean square values, $\langle\phi^2\rangle$ and $\overline{\phi^2}$, respectively, are also calculated using the above procedure. The instantaneous velocities U and V were ensemble averaged in this manner over 1000 effective cycles to obtain $\langle U\rangle, \langle V\rangle, \langle u^2\rangle, \langle v^2\rangle$ and $\langle uv\rangle$ as functions of the phase position θ_p. For more details of the whole procedure, see Ramaprian and Tu (1982).

Experimental Conditions

The nominal mean velocity U_0 and the amplitude of oscillation ϵ of the free stream were 90 cm/sec and 0.4 respectively. Two different frequencies, $f = \omega/2\pi = 0.5$ Hz and 2.0 Hz were studied. The turbulent bursting frequency f_b in the boundary layer, which can be regarded as a characteristic frequency of turbulence was estimated from the criterion of Rao, Narasimha and Badri Narayanan (1971), to vary from about 13 to 4.5 Hz from the first to the last measuring station. It is seen that the higher of the two oscillation frequencies is comparable to the bursting frequency, at least for the downstream-most station.

Preliminary surveys showed that U_e varied by less than 5% along the entire test section length and less than 2% in the range 90 cm $< x <$ 210 cm. The amplitude ϵ was also found to remain constant within the same limits. The freestream velocity modulation was sinusoidal everywhere along the test section with less than 1% total harmonic distortion, as confirmed by a Fourier analysis of the velocity signal. It was found from several spanwise traverses, that the boundary layer was acceptably two-dimensional over the central 30% of the span (corresponding to about 4δ), with respect to both mean and oscillatory properties. For example, these properties were uniform to within 2% in mean value and amplitude, and within 0.5 degree in phase in this region. All these initial experiments are documented in detail in Menendez and Ramaprian (1983).

Summary of Experimental Results

All the experimental data have been stored on magnetic tape in the format suggested by Dr. Lawrence Carr of NASA, Ames Research Center, for archival as AGARD data base. These data can be obtained by writing to either Dr. Carr or the author. Only some typical data are presented and discussed in this report.

Time-Mean Flow Properties

Figure 2 shows the variation of the time-mean values of $Re_\theta = U_0\overline{\theta}/\nu$, $H = \overline{\delta^*}/\overline{\theta}$ and $\overline{C}_f = 2\overline{\tau}_w/\rho U_0^2$ with $Re_x = U_0 x/\nu$, where $\overline{\delta^*}$ and $\overline{\theta}$ are the time-mean displacement and momentum thickness respectively. It is seen that the values of Re_θ and H are the same for the two unsteady flows but are significantly different from those for steady flow at the upstream stations. The time-mean wall shear stress, on the other hand, is only slightly affected at all stations by unsteadiness. In fact, the differences in $\overline{C}_f$ between the three flows are too small to be clearly distinguished from data scatter. The values of H and the slope dRe_θ/dRe_x also indicate that the unsteady and steady flows approach each other as Re_x increases.The data trend suggests that the initial differences between unsteady and steady flows are the result of shifts in the virtual origin. In fact, a careful study of the data indicated (see Menendez and Ramaprian 1983 for details) that the steady flow is not fully developed up to station 3, (possibly due to the ineffectiveness of the boundary-layer trip). It appears that the imposition of oscillation on the flow has the effect of promoting a faster evolution of the flow (especially the outer layer), into a a "standard" boundary layer. The evolutions of the mean velocity distributions in the usual inner and outer coordinates are shown in figures 3(a)-(d). The scaling velocity $\overline{u}_*$ used in these figures is obtained from the measured wall shear stress τ_w as $\overline{\tau}_w/\rho^{1/2}$ (using the fitted lines shown in figure 2b). The scaling length δ is obtained from a 3-parameter fit of the measured mean velocity distribution in the region $y^+ > 40$ to the Coles' "log+wake" distribution

$$\overline{U} = \sqrt{C_{f_e}}U_0[\frac{1}{\kappa}\ln(\frac{yU_0}{\nu}\sqrt{C_{f_e}}) + 5.5 + \frac{2\Pi}{\kappa}(3\eta^2 - 2\eta^3)] \qquad (3)$$

where $\kappa = 0.41, \eta = y/\overline{\delta}$ and $C_{f_e}, \eta, \overline{\delta}$, are the three free parameters. It is seen that the velocity distributions in the inner, as well as outer coordinates approach their respective steady-flow distributions towards the downstream locations. Once again, the departure observed in the upstream stations are the result of the different "histories" of the three flows and, hence, are specific to the apparatus. Some difference is still observed between the steady and unsteady flows at the most downstream station, at the oscillation frequency of 0.5 Hz but not at 2 Hz. This is, however, small and in view of the uncertainties in flow development, it is difficult to draw strong conclusions about the effect (if any) of oscillation on the time-mean flow.

The time-averaged turbulent stresses $\overline{u^2}$, $\overline{v^2}$ and $\overline{uv}$ are shown in figure 4 for the downstream-most station (station 5). The distributions at 2 Hz seem to be very nearly the same as in steady flow. The distributions at 0.5 Hz, however, show some departure from steady flow. In fact, a study of the data from all the stations indicated some correlation between the effect on these turbulence properties and the reduced frequency $\omega x/\nu$, with the effect being zero at very small and very large values of $\omega x/\nu$ and being a maximum around $\omega x/\nu = 5$ to 8. The authors have no satisfactory explanation for this observed trend. Other investigators have reported no effect of imposed unsteadiness on the time-averaged turbulence properties.

Oscillatory Motion

The response of the oscillatory velocity to to the imposed oscillation was everywhere found to be harmonic. The total harmonic distortion was less than 1 %. It is therefore adequate to consider only the fundamental component of the oscillatory velocity. The response of the other properties, however, may be significantly distorted. This is seen typically from figure 5 which shows the variation of the ensemble averaged wall shear stress $\langle \tau_w \rangle$ and the Reynolds shear stress $\langle uv \rangle$ during the oscillation cycle (the latter at three different points in the boundary layer) at station 5. However, Fourier analysis indicated that even in this case, the first harmonic is still the dominant one. Hence, only this component will be considered for discussion in this report. Complete information on all properties (including all the significant Fourier components) has, been stored on magnetic tape. In spite of the harmonic distortion in the $\langle uv \rangle$ variations, it is very clearly seen that $\langle uv \rangle$ is modulated very strongly near the wall (and so also is $\langle C_f \rangle$). The modulation in $\langle uv \rangle$ becomes weaker with increasing distance from the wall until it becomes zero in the outer part of the boundary layer resulting in a "frozen" turbulence structure in that region. This observation is in agreement with other experiments. Figure 5 also shows that there is a strong phase variation across the region where the amplitude modulation is significant. This region will henceforth be referred to as the "unsteady vortical layer".

Some typical results for the phase and amplitude distributions of $\langle U \rangle$, $\langle u^2 \rangle$ and $\langle uv \rangle$ are shown in figures 6 and 7. These data correspond to station 5. The amplitude of $\langle U \rangle$ exhibits the well known trend with a slight overshoot (7-8 % of the freestream amplitude). The extent of the region of amplitude variation, i.e., the thickness of the unsteady vortical layer decreases with frequency. Beyond this layer is a layer of constant amplitude or the so-called "slug-flow" layer. A quantitative measure of the thickness of the unsteady vortical layer is the distance y_m from the wall to the point of maximum amplitude. The quantity $\omega y_m^2/2\nu^{1/2}$ which is the ratio of y_m to the thickness of the laminar Stokes layer (or the unsteady viscous layer) has a value of about 10, at both frequencies studied, indicating that the unsteady effects to much larger distances in turbulent flow than in laminar flow. This result is in agreement with the pipe-flow data of Tu and Ramaprian (1983). The phase lead of $\langle U \rangle$, shown in figure 6 (b) also exhibits the well known trend of increasing lead towards the wall. However,

since data could not be obtained closer than 1 mm from the wall, the detailed manner in which the phase lead of the velocity approaches the phase lead of the wall shear stress cannot be understood from these measurements. This is not a serious drawback, however, since extensive near-wall data of high quality are available from the work of Jayaraman, Parikh and Reynolds (1982). The emphasis on the present experiments was in obtaining the Reynolds shear stress data.

The amplitude of oscillation of the turbulence properties $\langle u^2 \rangle$ and $\langle -uv \rangle$, normalized by $2\epsilon U_e^2$, is presented in figure 7. It can be shown, by considering small perturbations,that, with this nondimensionalization, the resulting quantities should be very nearly equal, in quasisteady flow at small ϵ, to the steady-flow values of $\overline{u^2}/U_e^2$ respectively (Shemer, Wygnanski and Kit 1985). Hence, the significant departure of the distributions in figure 7 from the steady-flow distributions of figure 4 suggests that the quantities $\langle u^2 \rangle$ and $\langle uv \rangle$ do not respond in a quasisteady manner, at both the oscillation frequencies. Further, it is seen that the region of significant variation in the amplitudes of these properties corresponds to the unsteady vortical layer observed in the case of $\langle U \rangle$. Beyond this region, the amplitude is essentially zero, indicating a state of frozen turbulence, in agreement with previous investigations.

The phase distributions of $\langle u^2 \rangle$ and $\langle uv \rangle$, relative to the freestream velocity, are presented in figures 7(c) and (d). These indicate phase lag in both cases, which tend to zero at or close to the wall (where the turbulence is produced), and increase to 360 degrees at the outer edge of the unsteady vortical layer (indicated by a vertical line, for $f = 2$ Hz). The data scatter observed beyond this layer, for $f = 2$ Hz, is a result of the Fourier analysis of the very small (spurious) modulation of velocity in that region and is not significant.

The amplitude and phase distributions of the turbulence properties are in general agreement with those measured by Ramaprian and Tu (1983) and Mizushina, Maruyama and Hirasawa (1975) in periodic pipe flow. Detailed studies showed that the phase lag of $\langle u^2 \rangle$ (and $\langle -uv \rangle$) increases approximately linearly through the unsteady vortical layer. The flow thus behaves as if the disturbance, imposed by the oscillation on the turbulence generated near the wall, diffuses outward with a nearly constant velocity. The distance travelled by the disturbance in one oscillation period due to this diffusion corresponds to the thickness of the unsteady vortical layer. If this thickness can regarded to be characterized by y_m (in order of magnitude) the present data suggest that the diffusion velocity is of the order of $\overline{u}_*$. Another significant point to be noted is that both $\langle u^2 \rangle$ and $\langle -uv \rangle$ are out of phase with $\langle U \rangle$ over most part of the unsteady vortical layer, a result which is in agreement with the observations of Ramaprian and Tu (1983). This points to the limitations of quasisteady eddy viscosity models that relate $\langle -uv \rangle$ to $\langle U \rangle$. A careful examination of figure 7 also shows that $\langle u^2 \rangle$ and $\langle -uv \rangle$ have a relative phase difference which varies across the unsteady vortical layer. This is, again, in agreement with the earlier results from pipe flow studies and shows that the turbulence structure is not in "equilibrium" during the oscillation cycle.

The mean value, as well as the amplitude and phase of the first harmonic of the skin-friction coefficient $\langle C_f \rangle$ as a function of oscillation frequency are shown in figure 8.

These data were obtained from a set of experiments in which the HFG was located at station 5 and the frequency of oscillation was varied from 0 to 2 Hz by using the sleeves designed for 0.5 Hz and 2 Hz. It was found that there was very little distortion in the wave form of the freestream velocity variation in spite of this off-design operation. A slight decrease in the time-mean value $\overline{C}_f$ (shown as a shaded band) is seen as the oscillation frequency is initially increased but the $\overline{C}_f$ values seem to level off at higher frequencies. The amplitude of $\langle C_f \rangle$ is normalized in the same manner as $\langle -uv \rangle$. Hence, the difference between the amplitude and the time-mean value is a measure of the departure from quasisteady behavior. It is seen that the oscillatory skin friction shows only a slight departure from quasisteady response at all frequencies. However, a monotonic and linear increase of phase lead of $\langle C_f \rangle$ with frequency is observed. The highest phase lead measured was about 38 degrees. These phase lead values are higher than the value of about 10 degrees observed by Ramaprian and Tu (1983) in pipe flow. They, however, seem to support the earlier experimental results on periodic boundary layers of Jayaraman, Parikh and Reynolds (1982) which suggest that the phase lead of $\langle \tau_w \rangle$ may eventually reach the laminar limit of 45 degrees at very high frequencies.

AN ASYMPTOTIC THEORY FOR THE PERIODIC TURBULENT BOUNDARY LAYER IN ZERO MEAN PRESSURE GRADIENT

The principal difficulty encountered in the analysis of turbulent flows both in steady and unsteady regimes, is the well known closure problem. A combination of a minimum of experimental information, dimensional analysis and singular perturbation theory has proved useful, in recent times, in providing quite general asymptotic results for large Reynolds numbers, in the form of similarity laws for many categories of steady turbulent shear flows (see Tennekes and Lumely 1980). The strength of this approach (and, perhaps, also its major limitation) is that it works on the open system of equations, thus avoiding the anomalies introduced by a specific turbulence model. While in the case of steady flows such analysis has merely reconfirmed already well-established experimental knowledge, it was used in the present work as a predictive tool to obtain similarity laws for unsteady turbulent flows. Some of these results were then verified using the available experimental information.

In analyzing the behavior of the velocity in unsteady (periodic) flows, one can search for similarity laws (e.g., law-of-the-wall, velocity-defect law, etc.) in the instantaneous (ensemble-averaged) profiles (e.g., Cousteix, Houdeville and Javelle 1981). This approach has not so far been very successful. In the present work, instead, the velocity profile is decomposed into its time-mean and oscillatory components, and each one of them was studied separately. The analysis and the results are briefly summarized below. More details can be found in Menendez and Ramaprian (1983, 1986).

The analysis is started from the ensemble-averaged unsteady turbulent boundary layer equations for an incompressible, two-dimensional flow (Patel and Nash 1971)

$$\frac{\partial \langle U \rangle}{\partial x} + \frac{\partial \langle V \rangle}{\partial y} = 0 \tag{4}$$

$$\frac{\partial\langle U\rangle}{\partial t}+\langle U\rangle\frac{\partial\langle U\rangle}{\partial x}+\langle V\rangle\frac{\partial\langle U\rangle}{\partial y}=-\frac{1}{\rho}\frac{\partial\langle p\rangle}{\partial x}+\nu\frac{\partial^2\langle U\rangle}{\partial y^2}+\frac{\partial\langle\tau\rangle}{\partial y} \tag{5}$$

$$-\frac{1}{\rho}\frac{\partial\langle p\rangle}{\partial x}=\frac{\partial U_e}{\partial t}+U_e\frac{\partial U_e}{\partial x} \tag{6}$$

The particular form of the periodic free-stream velocity given by (1) is assumed with both the time-mean value, U_0, and the relative amplitude of oscillation , ϵ ($\ll 1$) being constants. The assumption $\epsilon \ll 1$ allows a linear analysis in amplitude to be performed. This means that only motions at the forcing frequency are considered to be significant, while higher harmonic oscillations can be neglected. The advantage of the complex notation can, then be utilized, defining

$$U=\overline{U}+\epsilon\,U_1 e^{i\omega t} \tag{7}$$

$$V=\overline{V}+\epsilon\,V_1 e^{i\omega t} \tag{8}$$

$$\tau=\overline{\tau}+\epsilon\,\tau_1 e^{i\omega t} \tag{9}$$

and restating (1) as

$$U_e=U_0(1+\epsilon\,e^{i\omega t}) \tag{10}$$

Note that U_1, V_1 and τ_1 are all, in general, complex quantities.

In a steady turbulent boundary layer at large Reynolds number, there exist two distinctly different length scales of motion in the boundary layer, resulting in a double-layer structure; an outer layer characterized by the (local) mean boundary layer thickness, δ and an inner layer with length scale ν/u_* (Milikan 1938). Furthermore, as the boundary layer thickness, δ, is an ill-defined quantity, a thickness defined by

$$\Delta\equiv\int_0^\infty\frac{\overline{U}(U_0-\overline{U})}{U_0u_*}\,dy=\frac{U_0}{u_*}\theta \tag{11}$$

will be used instead, where θ is the momentum thickness. Note that the ratio of the two length scales defines the following Reynolds number:

$$R_*\equiv\frac{u_*\Delta}{\nu} \tag{12}$$

The velocity scale for both the layers is u_*. Hence the time scales are $t_0\equiv\Delta/u_*$ and $t_i\equiv\nu/u_*^2$ for the outer and inner layers, respectively (Tennekes and Lumely 1980).

In an unsteady turbulent boundary layer, the imposed oscillation introduces a third time scale, ω^{-1}, into the problem. Its relation to the outer and inner time scales can be described by the following two frequency parameters

$$\tilde{\omega}\equiv\frac{t_0}{\omega^{-1}}=\frac{\omega\Delta}{u_*}=\frac{\omega L}{U_0} \tag{13}$$

$$\alpha\equiv\frac{\omega^{-1}}{t_i}=\frac{u_*^2}{\omega\nu}=\frac{R_*}{\tilde{\omega}} \tag{14}$$

In addition, a third length scale, namely $\overline{u}_*/\omega$, appears, being associated with the imposed oscillation. This defines an "unsteady vortical layer" whose thickness bears to the outer and inner thicknesses the same relations as the corresponding time scales, and is thus described by the same parameters, i.e. $\tilde{\omega}$ and α, defined above.

Various flow regimes can be distinguished, according to the values of the foregoing parameters. For $\tilde{\omega} \leq 1$, the time scale $\omega^{-1} \geq t_0$ and hence, significant unsteady vorticity must be expected in the outer layer. In fact, the unsteady vortical layer is merged with the outer layer. On the contrary, since $\alpha = R_*/\tilde{\omega} \leq R_* \gg 1$, i.e., $\omega^{-1} \gg t_i$, the inner layer responds instantly to the excitation, i.e., in a quasisteady manner. This will be called the "low frequency regime". Note that, in particular case $\tilde{\omega} \ll 1$, the outer layer will also behave in a quasisteady manner.

The other extreme situation arises when $\tilde{\omega} \geq R_*$, i.e., $\alpha \leq 1$, in which case $\omega^{-1} \leq t_i$. Now, the unsteady vortical layer will be actually submerged in the inner (viscous) layer. The effects of unsteadiness are, therefore, significant in the inner layer. On the other hand, since $\omega^{-1} \ll t_0$, there is not enough time for the turbulent flow in the outer layer to respond to the imposed oscillation and hence this layer will move as a rigid body, i.e., it will perform "irrotational" or "slug-flow" oscillations. In fact, even the outer part of the inner layer may exhibit the slug-flow behavior. This situation will be named "very high frequency regime".

The situation $1 \ll \tilde{\omega} \ll R_*$ which lies between the two limiting cases described above, needs a more careful study. Since, under this condition, the inner and outer time scales are such that $t_i \ll \omega^{-1} \ll t_0$, one should expect that there will be quasisteady flow in the inner layer, while a slug-flow is present in the outer layer. Furthermore, the fact that $\nu/u_* \ll \overline{u}_* \ll \Delta$ in this flow, suggests that the unsteady layer lies between the outer and inner layers. Only in this unsteady layer are the unsteady vortical effects significant. In fact, it has been found useful in the analysis to divide the regime $1 \ll \tilde{\omega} \ll R_*$ into two distinct subregimes: an "intermediate-frequency regime", for which $1 \ll \tilde{\omega} \leq R_*^{1/2}$ (or equivalently $R_*^{1/2} \leq \alpha \ll R_*$) and a "high frequency regime", with $R_*^{1/2} \ll \tilde{\omega} \ll R_*$ (or equivalently $1 \ll \alpha \ll R_*^{1/2}$). Note that $\tilde{\omega} = R_*^{1/2}$ corresponds to the case $\omega^{1/2} = (t_0 t_i)^{1/2}$, i.e., the geometric mean of the outer and inner scales, for which $\tilde{\omega} = \alpha$.

Each of the above four frequency regimes has been analyzed by considering the appropriately normalized versions of equations (4-6) and using a combination of order of magnitude analysis and matched asymptotic expansions. This procedure is detailed in Menendez and Ramaprian (1983, 1986). The procedure results in the identification of asymptotic similarity laws that describe the variation of the oscillatory velocity in the different layers in the different frequency regimes.

For a free-stream velocity given by (1), the longitudinal velocity component can be written as

$$U = \overline{U} + \epsilon \left(U_{11} \sin \omega t - U_{12} \cos \omega t \right) \tag{15}$$

where U_{11} and U_{12} are, respectively, the in-phase and out-of-phase components of the oscillatory motion. The similarity laws for U_{11} and U_{12} resulting from the above analysis are summarized in Table 1. They are valid in the asymptotic limit for $R_s \to \infty$. Hence they should be referred to as "weak" similarity laws (Yajnik 1970), in the sense that they hold only to the lowest order asymptotic analysis. Deviations from these asymptotic laws should be expected, in practice, at finite values of R_s.

The concept developed for zero time-mean pressure gradient flows admits a relatively simple extension to other types of flow. An extension of the present theory to boundary layers in nonzero time-mean pressure gradient, as well as to fully developed flow in channels and pipes is also described in Menendez and Ramaprian (1983).

Experimental Results in the Light of the Theory

The above theory has been applied to the present as well as previously reported experimental results of periodic turbulent shear flows. Detailed comparisons are reported in Menendez and Ramaprian (1983, 1986). Only a few typical comparisons are shown in figures. Table 2 shows the most relevant parameters for the present data at each station and for the two oscillating frequencies studied. It is observed that the majority of the situations correspond to the intermediate-frequency regime. The remaining ones are in the transition range between the low and intermediate-frequency regimes. Therefore, they are expected to exhibit, to some extend, the main characteristics of both regimes. Table 3 shows a list of the other experiments, together with their most relevant parameters.

The cases in the low or low/intermediate-frequency regime must be expected to exhibit the "logarithmic law", (see Table 1). Figure 9(a) presents the in-phase oscillatory component, U_{11}, in the inner coordinates, for experiments M1, M5, CA, T1 and J1. Data corresponding to intermediate and intermediate/high-frequency regimes (experiments J2, J3 and J4) are also presented in this figure. Also shown is the line corresponding to the universal logarithmic law for the mean velocity profile in steady flow. Its slope is used as reference. It is readily observed that, there is a range in which the in-phase component varies logarithmically and with the same universal slope, as predicted by the theory. Towards the outer edge, a "wake component" can be identified as for the steady-flow mean velocity profile, but extending deeper into the boundary layer. Note that this wake component is very strong for experiment J1 due to the time-mean adverse pressure gradient. This reduces considerably the extent of the logarithmic region (situated around $y^+ \cong 30$). The corresponding out-of phase component U_{12}, is shown in figure 9(b). It is seen that, in fact, there is a region of constant U_{12} for the low and low-intermediate frequency experiments, in agreement with Table 1. This value generally corresponds to the minimum of each distribution, except for experiment J1 for which the region of constant value seems to behave like a "saddle point". These results show that, like the time-mean flow, the oscillatory motion in the outer layer for the low-frequency regime depends strongly on the particular flow conditions.

Table 1 shows that in the intermediate-frequency regime, there must exist an outer region of "slug" flow. That this is, in fact, the case has been confirmed by the

present experimental data as well as the data from other experiments. Immediately next to this layer, and closer to the wall, an intermediate unsteady vortical layer develops where a "velocity-defect law" (see also Table 1) must be satisfied. Figures 10(a) and 10(b) show the in-phase and out-of-phase velocity components, respectively, for all the present experimental data, plotted in the coordinates corresponding to the unsteady vortical layer. The error in the asymptotic results is of order $(\ln R_*)^{-1}$, which corresponds approximately to $\pm$ 0.2 (see Table 2). It is therefore concluded, that the collapse is reasonably good for the truly intermediate-frequency cases, in agreement with the theory. Deviations occur for the transitional low/intermediate-frequency cases, specially for the out-of-phase component and closer to the outer edge of unsteady layer. In these cases, the slug-flow region has nearly disappeared, so the unsteady layer extends practically up to the edge of the boundary layer. Hence, the deviations must result from the interaction with the free-stream. In all the cases, the scatter for the out-of-phase component is much larger than for the in-phase component. This is, as already mentioned, due to larger experimental errors in the measurement of U_{12}. It is significant to note that the location of the peak in the in-phase component, which is a measure of the extent of the unsteady vortical layer, corresponds to $\hat{y} \cong 1$.

The above discussion permits one to construct a general, though still speculative, picture of how the oscillatory components behave when the frequency parameter $\tilde{\omega}$ increases, as shown in figure 11. This figure refers to the case of a zero time-mean pressure gradient boundary layer. It is observed that there is a continuous transition between the "log + wake" profile for the low-frequency regime and the Stokes (viscous) solution for the very high-frequency regime.

Generalization of the Theory to Other Flow Properties

Though the theory has been developed for the oscillatory velocity components, the idea can be extended to analyze other flow properties also. If the in-phase and out-of-phase components of the turbulence properties, namely $\langle u^2 \rangle$, $\langle v^2 \rangle$, and $\langle uv \rangle$, are defined with complete analogy with those for the velocity, they must scale with $\overline{u}_*^2$. To be consistent with earlier definitions they are normalized with $2\overline{u}_*^2$. Their distributions in the unsteady-layer coordinates, for the present experiments, are shown in figures 12(a), (b), (c). With the same admitted error as for the velocity ($\pm$ 0.2), the data for the in-phase component collapse fairly well for all the quantities, except for $\langle u^2 \rangle$ in the outer part of the unsteady layer. Deviations occur there for the transitional low/intermediate-frequency cases. As in the case of velocity, this must be attributed to interactions with the free stream, including some feedback of free-stream turbulence into the boundary layer. Less satisfactory is the performance of the out-of-phase components, especially in the near-wall region. This can be due to higher sensitivity of the turbulent quantities to the value of α. The agreement improves when moving outwards, except for $\langle u^2 \rangle$, for which the same remarks apply as for the in-phase component. Note that the best data collapse is obtained for $\langle uv \rangle$.

As in the case of the turbulence properties, the in-phase and out-of-phase components of the wall shear stress $\langle \tau_w \rangle$ must scale with u_*^2. Figure 13 presents the amplitude phase of oscillation of the wall shear stress as a function of the frequency parameter $\tilde{\omega}$.

Included are the measurements at all stations and at all frequencies. The collapse is satisfactory within the experimental error estimated to be $\pm$ 0.08. It is observed that the amplitude does not vary drastically with $\tilde{\omega}$. There possibly exists a mild minimum around $\tilde{\omega} \cong 30$ to 35. The variation of the phase of $\langle \tau_w \rangle$ with the frequency $\tilde{\omega}$ exhibits an approximately linear trend, though the distribution should eventually reach the 45-degree line for large $\tilde{\omega}$.

THEORY OF THE USE OF SKIN FRICTION GAGE

The conventional calibration procedure for the flush-mounted hot film, when used as a skin-friction gauge, fails in high frequency periodic flows. A theory for the use of this gauge in unsteady flows has been developed. This theory leads to the general calibration formula

$$\tau_w = (AE^2 + B)^3 + c_1 \frac{dU_e}{dt} \frac{1}{AE^2 + B} + c_2 A \frac{dE^2}{dt} \tag{16}$$

which replaces the conventional calibration formula:

$$\tau_w^{1/3} = AE^2 + B, \tag{17}$$

where E is the anemometer output voltage, A and B are the conventional calibration constants and c_1, c_2 are constants that can be obtained by a special calibration procedure. The usefulness and limitations of the proposed formula for laminar as well as turbulent flows have been established by comparing its accuracy against exact numerical solutions of the unsteady thermal and hydrodynamic boundary layers over the film. The work is described in detail in Menendez and Ramaprian (1984, 1985). The present theory has been developed under certain restrictive assumptions, described in the above references. While these assumptions are generally valid for most of the applications of the skin-friction gauge, it is necessary to verify that these conditions are satisfied before applying the theory to any specific problem.

A procedure for the calibration of the probe has also been developed. Also a simplified linearized version of the formula (16) has been suggested. This extends the use of the skin-friction gauge to the measurements of the energy spectrum of wall-shear-stress fluctuations in steady turbulent flows, in which such fluctuations are small relative to the mean value.

While the dynamic effects of heat transfer to the fluid have been fully taken into account in the present theory, a limitation of the present theory is that dynamic effects on the substrate heat transfer have been ignored, albeit with some justification. This aspect needs further theoretical study. It is also very important to conduct experiments that can lead to an assessment of the accuracy of the calibration procedure recommended in this paper. For example, this procedure can be tested by using it for measuring the instantaneous wall shear stress in a laminar periodic boundary layer, for which the exact solution can be obtained analytically or numerically. Unfortunately, because of experimental limitations, such test could not be conducted by the authors.

It is also possible to verify the accuracy of the present procedure if alternative independent techniques for measuring wall shear stress in unsteady turbulent flows become available in the future.

COMPUTATIONAL STUDIES

The computational studies performed during the period of the present contract included:

1. the development of "wall functions" (see Patankar and Spalding (1968)
2. the development of a calculation procedure for unsteady turbulent boundary layers, based on a 2-equation model of turbulence.

The wall functions appropriate for a $k-\epsilon$ type model were obtained for unsteady boundary layers from the experimental data and the theoretical frame work described in the previous sections. These functions were obtained in the form of algebraic expressions that fitted the near-wall data in figures 10,11 and 12. Details of this procedure and the recommended wall functions are described in Menendez and Ramaprian (1984).

A finite-difference calculation procedure based on the well known $k-\epsilon$ model of turbulence was developed for the prediction of unsteady turbulent boundary layers. The method is an extension of the one-equation procedure developed earlier by Menendez and Ramaprian (1981, 1984) and has been adapted for use with wall functions. The procedure was used for the prediction of the present experiments in zero pressure gradient. Some typical results are shown in figures 14 and 15. These refer to the amplitude and phase of the oscillatory velocity, and the in-phase and out-of-phase components of the Reynolds shear stress. Results for both oscillation frequencies of 0.5 Hz and 2 Hz are shown. The results shown correspond to stations 2,3,4 and 5 and are compared with the experimental data. The initial conditions for the calculation were matched with the experimental data at station 1. Only the finite-difference solutions are shown and hence these do not extend to the wall. The distributions near the wall can be obtained from the wall functions.

The agreement between the predictions and measurement can, at best, be described as moderate. The failure of the calculation procedure to give better predictions is most likely due to the inadequacy of the turbulence model to describe the turbulent flow at intermediate to high frequencies of oscillation. Inadequacy of the wall functions and numerical deficiencies may also be partly responsible but are unlikely to be the major factors. More effort is obviously needed to improve our capability to predict unsteady turbulent boundary layers.

EXPERIMENTS IN ADVERSE PRESSURE GRADIENT

These experiments were performed to obtain a comprehensive data base on periodic turbulent boundary layers characterized by a significant degree of flow reversal during the oscillation cycle. These data compliment those obtained by Cousteix,

Houdeville and Javelle (1981), Simpson, Shivaprasad and Chew (1983), Simpson and Shivaprasad (1983), and Jayaraman, Parikh and Reynolds (1982). The present experiments provide, in particular, data on the Reynolds shear stress obtained from two-component LDA and wall shear stress obtained from using a heat-flux gage (corrected for unsteady effects) at intermediate to large values of reduced frequency. The amplitude and phase of the freestream velocity were maintained approximately constant over a significant distance along the flow. Two sets of experiments were performed. In one of these, a "mild" adverse pressure gradient was set up such that an equilibrium boundary layer would be produced in steady flow. In the other experiment, a stronger adverse pressure gradient was maintained over a short downstream portion of the flow. It was the intention to produce zero mean skin friction in this flow. Unfortunately, this could not be achieved due to apparatus size limitations. It was, however, possible to produce flow reversal during a substantial part of the oscillation cycle, in this experiment.

Modification of the Test Section

The desired pressure gradient was set up in each experiment by appropriately modifying the shape of the top wall of the test section. In the first case, this shape was calculated by imposing the condition that the Clauser parameter β defined as:

$$\beta = -\frac{\delta^*}{u_*^2}\frac{dU_e}{dx}$$

should remain constant in steady flow in the downstream part of the test section. The actual constraint imposed on β is shown in figure 16. This distribution of β, along with the appropriate initial conditions, was used in an inverse procedure to calculate the required top wall geometry for obtaining an equilibrium boundary layer in steady flow. Head's entrainment method was used for the boundary-layer calculation in this procedure. The resulting top-wall geometry and the measurement locations are shown in figure 17(a). The measured values of the boundary-layer parameters H and Π are shown in table 4. It is seen that the steady boundary layer is nearly in equilibrium over the region x=1.42 to 2 meters.

In the second experiment, the shape of the top wall was further modified in the downstream section in order to obtain a higher pressure gradient. The upstream part of the test section remained the same as in the first experiment, but a 50 cm long flat plate set back at an angle of incidence of 12 degrees was used to replace the downstream part of the upper wall, as shown in figure 17(b). The boundary layers over a length of 5 cm along the top and side walls just upstream of the plate was withdrawn through perforations in the wall to prevent flow-separation along these walls. The arrangement for the withdrawal of the boundary layers is shown in figure 18. The dimensions of the various components of this system were calculated from numerically modelled unsteady flow through the system, driven by the oscillating pressure inside

the tunnel.The numerical calculations indicated that the (two-dimensional) boundary layer would separate inside the tunnel at all flow rates through the tunnel. Actual measurements, however, showed that flow separation occurred only at very low flow rates in steady flow. In the unsteady flow, flow reversal was found to occur only during a portion of the oscillation cycle. Stronger pressure gradients could not be set up because of the limited size of the tunnel.

Experimental Conditions

All the initial experiments necessary for documenting the flow quality were performed in exactly the same manner as in the zero-pressure-gradient (ZPG) experiments. After these initial tests, regular experiments were performed at two oscillation frequencies, namely 0.5 Hz and 2 Hz with the mild pressure gradient and at only one frequency of 0.5 Hz with the stronger pressure gradient. The average amplitude of oscillation was about 0.4 of the mean velocity in all the cases. The variations of amplitude and phase of the free stream velocity along the entire test section are shown for the mild-pressure-gradient experiment in figures 19(a)-(d). It is seen that while these variations are not large(< 5 % in amplitude and within $\pm$ 2.5 % in phase) over the downstream half of the test section, there is a clear indication of spatial periodicity in the variations. This is due to the presence of such a spatial periodicity in the displacement thickness (as observed by Cousteix et al 1981), which is transferred to the free stream by the interaction between boundary layer and the core flow.

Summary of Results

As in the case of the ZPG results, all the experimental data have been archived on tape and is available to any interested user. Only a few typical results are presented here. A more elaborate presentation and discussion of the data can be found in the forthcoming Ph.D. thesis of B. Gajdeczko. The data presented here correspond to the mean and fundamental Fourier component only. Higher harmonics (information on which is available on tape) were not found to be significant in the case of velocity. While these are significant in the case of wall shear and turbulent stresses, the fundamental component is still the most dominant one even in these cases. Results for mild pressure gradient are summarized first. These are followed by the results for the stronger pressure gradient.

Results for Mild Pressure Gradient

Time-mean flow

The time-mean velocity distributions in steady and unsteady flows are shown in figures 20(a),(b),(c). It is seen that at this equilibrium mild pressure gradient, the time-mean velocity is not affected by the imposed unsteadiness. Effects due to the shift in the virtual origin, observed in ZPG flow are absent here, apparently because the rapid changes in the tunnel cross section cause the transition to be fixed at the same location in both steady and unsteady flows.

The data on long-time averaged turbulent shear stress are shown in figures 21(a)-(d). This is seen to be affected by oscillation, especially in the downstream locations and the higher oscillation frequency. Similar results were obtained for the other Reynolds stress components also.

Oscillatory flow

The amplitude and phase of the oscillatory velocity(fundamental component) are shown in figures 22 and 23. These properties exhibit very complex distributions across the boundary layer. The most noticeable feature of these distributions is the appearance of a two-layer structure, especially in the more downstream locations and a lack of self-similarity. The amplitude variations are small at the higher frequency, as expected. The lack of similarity is perhaps due to the existence of a spatial periodicity in the direction. Such periodicity could not be observed clearly in the present boundary-layer data, mainly because of the sparse spacing of the measuring stations along the tunnel. The phase distributions also indicate a two-layer structure, with the outer layer exhibiting significant phase lags.

The skin-friction variation during the oscillation cycle is shown in figures 24 (a)-(d). These data were obtained from the skin-friction gage, using the procedure described earlier. While the data around $\langle C_f \rangle \approx 0$ are suspect, it is expected that the results for $\langle C_f \rangle \geq 0.005$ are of acceptable accuracy. Furthermore, these figures show that the present procedure allows negative values of $\langle C_f \rangle$ to be measured.

Finally, figures 25 and 26 show the distributions of the amplitude and phase of $\langle uv \rangle$ across the boundary layer. Comparison of the amplitude distributions with the distributions of $\overline{uv}$ in figure 21 shows that, except at station 2 for 0.5 Hz, the response of the turbulent stress significantly departs from a quasisteady behavior. The smaller modulations of $\langle uv \rangle$ at higher values of reduced frequency and the two-layer structure of the flow in the downstream region of the flow are quite apparent from the figures. The phase distributions of $\langle uv \rangle$ in figure 26 show abrupt jumps. These are associated with the transition between the two layers of the multilayered structure. The phase jumps suggest that the two layers are driven by independent mechanisms. The generation of

maximum turbulent energy far away from the wall may be the probable cause of the double-layer structure. However, no definitive explanation can be given at this time.

Results for Strong Adverse Pressure Gradient

The mean flow conditions for this experiment are shown in table 4. It can be seen that the data have been obtained at close spacings in the range x=1.35 to 1.70 meters. Over this short region, the shape factor increases from 1.48 to 1.70 (compared to about 1.52 in the first experiment). The wake parameter Π also is correspondingly larger in this case. The unsteady flow was found to exhibit reversal over a greater fraction of the oscillation cycle in this experiment. As already mentioned, only one oscillation frequency, namely 0.5 Hz was studied in this case. Typical results are presented in figures 27-32.

The results are qualitatively similar to those at the milder pressure gradient. It is, therefore, not necessary to discuss them in detail. The only important points that need to be mentioned are:

1. The time-mean velocity profiles seem to indicate a slight effect of imposed oscillation (The rather large effect seen at x=155 cm cannot be explained except as being probably due to measurement errors).

2. The long-time averaged Reynolds shear stress shows a significant effect of imposed unsteadiness in the downstream stations

3. The amplitude of oscillatory velocity exhibits even more complex distributions that vary from station to station. The phase variations are qualitatively similar to those in mild pressure gradient but exhibit stronger phase lags in the outer layer.

4. The amplitude and phase of $\langle uv \rangle$ exhibit trends similar to those in mild pressure gradient. In fact, there is a stronger evidence of a two-layered structure in this flow.

CONCLUDING REMARKS

The main achievements of the research work performed under this contract can be summarized as follows.

1. An extensive set of data have been obtained on periodic turbulent boundary layers in zero as well as adverse pressure gradient, from experiments performed in a specially designed water tunnel. These data include Reynolds stresses and wall shear stress. The initial and boundary conditions are all well documented.

All the data have been archived on magnetic tape in a "standard" format and are available to the research community.

2. A comprehensive theory has been developed for periodic turbulent boundary layers. This theory leads to the identification of several similarity laws for unsteady turbulent boundary layers. These laws have, in turn, been used to develop "wall functions" needed in many boundary-layer calculation codes.

3. A theory has been developed for the use of flush-mounted hot-film gages to measure skin-friction in unsteady flows.

4. The large-amplitude periodic turbulent boundary layer in time-mean adverse pressure gradient exhibits a two-layer structure. This structure is not well understood at this time. Work in this direction will be continued as a part of the Ph.D. dissertation of B. Gajdeczko. His thesis which is expected to be completed by about June 1987 will also contain more details on the adverse-pressure-gradient boundary- layer experiments, than have been presented in this brief report.

REFERENCES

Cousteix, J., Houdeville, R. and Javelle, J. 1981, Response of a Turbulent Boundary Layer to a Pulsation of the External Flow with and without Adverse Pressure Gradient, IUTAM Symposium on Unsteady Turbulent Shear Flows, Tulouse, France, 5-8 May.

Jarayaman, R., Parikh, P. and Reynolds, W.C. 1982, An Experimental Study of the Dynamics of an Unsteady Turbulent Boundary Layer, Technical Report TF-18, Dept. of Mech. Eng., Stanford University.

Menendez, A.N. and Ramaprian, B.R. 1983, On the Measurement of Skin Friction in Unsteady Flow Using a Flush Mounted Hot Film Gage, Iowa Institute of Hydraulic Research Report No. 200.

Menendez, A.N. and Ramaprian, B.R. 1983, Study of Unsteady Turbulent Boundary Layers, Iowa Institute of Hydraulic Research Report No. 270.

Menendez, A.N. and Ramaprian, B.R. 1985, The Use of Flush Mounted Hot-Film Gauges to Measure Skin Friction in Unsteady Boundary Layers, *J. Fluid Mech.*, 161, 139-159.

Menendez, A.N. and Ramaprian, B.R. 1986, Periodic Turbulent Boundary Layers: A General Theory and Comparison with Experiments, submitted to the *J. Fluid Mech.*

Milikan C.B. 1938, Proc. 5th Int. Cong. Appl. Mech., Cambridge, MA., 386.

Mizushina, T., Maruyama, T. and Hirasawa, H. 1975, Structure of the Turbulence in Pulsating Pipe Flows, J. of Chem. Eng. of Japan, 8, No. 3, 210-216.

Ramaprian, B.R. and Tu, S.W. 1982, Study of Periodic Turbulent Pipe Flow, Iowa Institute of Hydraulic Research Report No. 238.

Rao, K.N., Narashima, R. and Badri Narayanan, M.A. 1971, The Bursting Phenomena in a Turbulent Boundary Layer, *J. Fluid Mech.*, 48, 339-352.

Shemer, L., Wygnanski, I. and Kit, E. 1985, Pulsating Flow in Pipe, *J. Fluid Mech.*, 131, 319-340.

Simpson, R.L., Shivaprasad, B.G. and Chew, Y.T. 1983a, The Structure of Separating Turbulent Boundary Layer. Part 4. Effects of Periodic Free-Stream Unsteadiness, *J. Fluid Mech.*, 127, 219-262.

Simpson, R.L. and Shivaprasad, B.G. 1983b, The Structure of Separating Turbulent Boundary Layer. Part 5. Frequency Effect on Periodic Unsteady Free-Stream Flows, *J. Fluid Mech.*, 131, 319-340.

Tennekes, H. and Lumely, J.L. 1980, A First Course in Turbulence, MIT Press.

Yajnik, K.S. 1970, Asymptotic Theory of Turbulent Shear Flows, *J. Fluid Mech.*, 42, 411-427.

Participating Scientific Personnel

1. Dr. B.R. Ramaprian, Principal Investigator
2. Dr. F. Stern, Coprincipal Investigator
3. Dr. A.N. Menendez, Graduate Research Assistant
4. Mr. B. Gajdeczko, Graduate Research Assistant

Degrees Awarded

A.N. Menendez Received Ph.D. in Mechanical Engineering. 1983

B. Gajdeczko Expected to receive Ph.D. in 1987

Publications and Technical Reports resulting from the Contract

Publications

Menendez, A.N. and Ramaprian, B.R. 1983. Calculation of unsteady boundary layers. *Proc. of the Third Int. Conf. on Num. Methods in Laminar and Turbulent Flow.* Univ. of Washington, Seattle, Aug. 8-11.

Tu, S.W. and Ramaprian, B.R. 1984. Quasisteady modeling of periodic turbulent pipe flows. *AIAA Journal.* Vol.22, No. 10, pp.1356-1357.

Menendez, A.N. and Ramaprian, B.R. 1984. Prediction of periodic boundary layers. *Int. J. for Num. Methods.* Vol.4, pp. 781-800.

Ramaprian, B.R. 1984. A review of experiments in periodic turbulent pipe flow. Keynote paper presented at the *ASME Energy Sources Technology Conf. and Exhibition.* New Orleans, Feb. 12-17.

Menendez, A.N. and Ramaprian. 1984. Quasisteady modeling of unsteady turbulent boundary layers. paper presented at *The Sixteenth IUTAM Conference*, Lyngby, Denmark, Aug 19-25.

Ramaprian, B.R., Tu, S.W. and Menendez, A.N. 1985. Periodic turbulent shear flows. *Turbulent Shear Flows* 4. ed. L.J.S. Bradbury, F. Durst,B.E. Launder and J.H. Whitelaw. Springer-Verlag, Berlin, pp.301-310.

Menendez, A.N. and Ramaprian, B.R. 1985. The use of flush-mounted hot-film gages to measure skin friction in unsteady boundary layers. *J. Fluid Mech.* Vol.151, pp. 139-159.

Menendez, A.N. and Ramaprian, B.R. 1985. Wall functions for unsteady turbulent boundary layers. *Proc. of the Fourth Int. Conf. on Num. Methods in Laminar and Turbulent Flow*, Swansea, U.K.

Ramaprian,B.R. 1985. Experimental techniques in unsteady turbulent flows. Invited paper presented at the Forum on Unsteady Flows in Biological Systems, *ASME Joint Meeting of teh App. Mech. Bioengrg. and Fluids Engrg. Division*, Albuquerque, NM, June 24-26.

(Menendez, A.N. and Ramaprian, B.R. 1986. The unsteady turbulent boundary layer: A general theory and comparison with experiments. Paper submitted to the J. Fluid Mech.)

Technical Reports

Menendez, A.N. and Ramaprian, B.R. 1983 Study of Unsteady Turbulent Boundary Layers. IIHR Rep. No. 270, The Univ. of Iowa, Iowa City, December. (Also the Ph.D. Thesis of A.N. Menendez)

Menendez, A.N. and Ramaprian, B.R. 1984. On the Measurement of Skin Friction in Unsteady Boundary Layers Using a Flush-Mounted Hot-Film Gage. IIHR Rep. No. 272, The Univ. of Iowa, Iowa City, April.

Table 1

Similarity Laws for Periodic Turbulent Boundary Layers

Layer / Regime	Inner	Unsteady	Outer
Low-frequency	$\frac{U_{11}}{u_*} = f_{11}(y^+)$ $\frac{U_{12}}{u_*} = f_{12}(y^+)$ with limits $f_{11} \to \frac{1}{k} \ln y^+ + B_{11}$ $f_{12} \to B_{12}$ as $y^+ \to \infty$	$\frac{U_{11}-U_0}{u_*} = F_{11}(\eta;\tilde{\omega})$ $\frac{U_{12}}{u_*} = F_{12}(\eta;\tilde{\omega})$ with limits $F_{11} \to \frac{1}{k} \ln \eta + D_{11}$ $F_{12} \to D_{12}$ as $\eta \to 0$	
Intermediate-frequency	$\frac{U_{11}}{u_*} = f_{11}(y^+)$ $\frac{U_{12}}{u_*} = f_{12}(y^+)$	$\frac{U_{11}-U_0}{u_*} = F_{21}\left(\frac{\omega y}{u_*}\right)$ $\frac{U_{12}}{u_*} = F_{22}\left(\frac{\omega y}{u_*}\right)$	
High-frequency	$\frac{U_{11}}{U_0} = a_1 y^+$ $\frac{U_{12}}{U_0} = a_2 y^+$		$U_{11} = U_0$ $U_{12} = 0$
Very high-frequency	$\frac{U_{11}}{U_0} = 1 - e^{-\eta_s} \cos \eta_s$ $\frac{U_{12}}{U_0} = -e^{-\eta_s} \sin \eta_s$ with $\eta_s = \frac{y^+}{\sqrt{2\alpha}} = \sqrt{\frac{\omega}{2\nu}}\, y$		

Note: F_{11}, F_{12}, f_{11}, f_{12}, F_{21}, and F_{22} are unknown functions, and D_{11}, D_{12}, B_{11}, B_{12}, a_1 and a_2 are unknown constants.

Table 2

Characterization of the Experiments for the Zero Pressure Gradient

Experiment	M1	M2	M3	M4	M5	M6	M7	M8	M9	M10
Station No.	1	2	3	4	5	1	2	3	4	5
f(Hz)			0.5					2		
θ(cm)	0.213	0.244	0.283	0.380	0.463	0.213	0.244	0.283	0.380	0.463
E	0.0420	0.0419	0.0414	0.0400	0.0392	0.0420	0.0419	0.0414	0.0400	0.0392
Δ(cm)	5.07	5.83	6.84	9.49	11.8	5.07	5.83	6.84	9.49	11.8
L(cm)	121	139	165	237	301	121	139	165	237	301
R_*	1920	2200	2550	3420	4170	1920	2200	2550	3420	4170
$R_*^{1/2}$	43.8	46.9	50.5	58.5	64.5	43.8	46.9	50.5	58.5	64.5
$\tilde{\omega}$	4.21	4.85	5.76	8.28	10.5	16.8	19.4	23.0	33.1	42.1
α	456	453	442	413	396	114	113	111	103	99.0
Freq. Regime	Low/Int	Low/Int	Low/Int	Low/Int	Int	Int	Int	Int	Int	Int

Table 3

Characterization of Other Experimental Studies

Reference	Cousteix, Houdeville & Desopper (1977)	Tu & Ramaprian (1983)		Jarayaman, Parikh & Reynolds (1982)				Acharya & Reynolds (1975)	Binder & Kueny (1981)
Time-Mean Flow	Zero Pr. Gr.	Pipe Flow		Adverse Pr. Gr.		Strong Adverse Pr. Gr.		2-D Channel Flow	2-D Channel Flow
Fluid	Air	Water		Water		Water		Air	Water
Expt. Designation	CA	T1	T2	J1	J2	J3	J4	AR	BK
f(Hz)	43	0.5	3.6	0.1	2	0.1	2	24	0.66
U_∞ or U_o (cm/s)	3360	108.9	113.7	69.54	69.54	54.90	54.90	667.5	17.5
ϵ	0.35	0.64	0.15	0.05	0.05	0.25	0.25	0.036	0.056
u_* (cm/s)	139	4.95	4.83	2.42	2.42	1.46	1.46	31.4	0.80
θ or h or R(mm)	0.960	25.4	25.4	5.73	5.73	12.1	12.1	31.75	50
R_*	2150	1260	1230	3980	3980	6660	6660	605	400
$R_*^{1/2}$	46.4	35.5	35.0	63.1	63.1	81.6	81.6	24.6	20
$\tilde{\omega}$	4.51	1.61	11.9	4.27	85.5	19.6	392	16.4	26.0
α	477	779	103	932	46.6	339.8	77.9	37.0	15.4
Freq. Regime	Low/Int	Low	Int	Low/Int	Int	Int	Int/High	Int.	Int.

Table 4
Mean-Flow Properties for the Adverse Pressure Gradient

x(m)	$\bar{U}_e$(cm/s)	δ(cm)	δ^*(cm)	θ(cm)	Re_{δ^*}	Re_θ	H	u_*(cm/s)	Π
Mild Adverse Pressure Gradient									
Steady Flow									
0.72	119.5	2.53	0.50	0.34	5990	4048	1.48	4.165	1.37
0.92	111.1	3.24	0.67	0.45	7463	4970	1.50	3.676	1.61
1.42	98.7	4.69	1.06	0.68	10261	6608	1.51	2.968	1.95
1.72	96.2	6.71	1.47	0.96	14095	9229	1.53	2.876	2.06
2.02	91.6	8.41	1.83	1.20	16736	10941	1.53	2.696	2.09
f=0.5 Hz									
0.72	114.2	2.65	0.56	0.37	6410	4221	1.52	3.826	1.64
0.92	113.1	3.58	0.81	0.52	8114	5861	1.56	3.495	2.04
1.42	99.3	5.93	1.37	0.88	13588	6671	1.57	2.890	2.34
1.72	95.8	7.08	1.54	1.01	14680	9655	1.52	2.864	2.03
2.02	91.9	8.23	1.87	1.21	17135	11053	1.55	2.628	2.32
f=2.0 Hz									
0.72	110.3	2.42	0.51	0.34	5631	3702	1.52	3.750	1.58
0.92	101.6	3.46	0.76	0.76	7659	4995	1.56	3.272	1.82
1.42	91.6	6.23	1.47	1.47	13450	8485	1.59	2.620	2.44
1.72	90.0	7.89	1.94	1.94	17395	10779	1.61	2.430	2.79
2.02	84.4	9.63	2.34	2.34	19677	12280	1.60	2.271	2.71
Strong Adverse Pressure Gradient									
Steady Flow									
1.35	100.2	6.10	1.25	0.68	10665	8452	1.47	3.254	1.47
1.40	95.7	5.18	1.21	0.77	11577	7330	1.58	2.816	2.31
1.45	92.2	5.58	1.36	0.83	12465	7653	1.63	2.608	2.60
1.50	90.0	6.23	1.54	0.94	13828	8419	1.64	2.482	2.76
1.55	87.8	6.58	1.72	1.02	15003	8894	1.69	2.294	3.19
1.60	86.6	6.92	1.84	1.08	15895	9306	1.71	2.206	3.39
1.65	85.4	7.19	1.92	1.12	16350	9543	1.71	2.159	3.44
1.70	85.0	7.70	2.04	1.20	17248	10137	1.70	2.159	3.37
f=0.5 Hz									
1.35	97.7	6.51	1.54	0.97	14970	9462	1.58	2.769	2.48
1.40	94.6	6.31	1.63	0.98	15392	9247	1.67	2.549	3.09
1.45	91.4	6.84	1.80	1.07	16426	9760	1.68	2.352	3.28
1.50	89.7	7.62	2.08	1.21	18607	10813	1.72	2.204	3.65
1.55	85.7	7.76	2.08	1.22	17795	10433	1.71	2.159	3.44
1.60	84.9	8.34	2.28	1.32	19282	11203	1.72	2.076	3.67
1.65	81.7	8.68	2.39	1.38	19440	11254	1.73	1.985	3.73
1.70	81.7	8.83	2.44	1.41	19862	11441	1.74	1.975	3.77

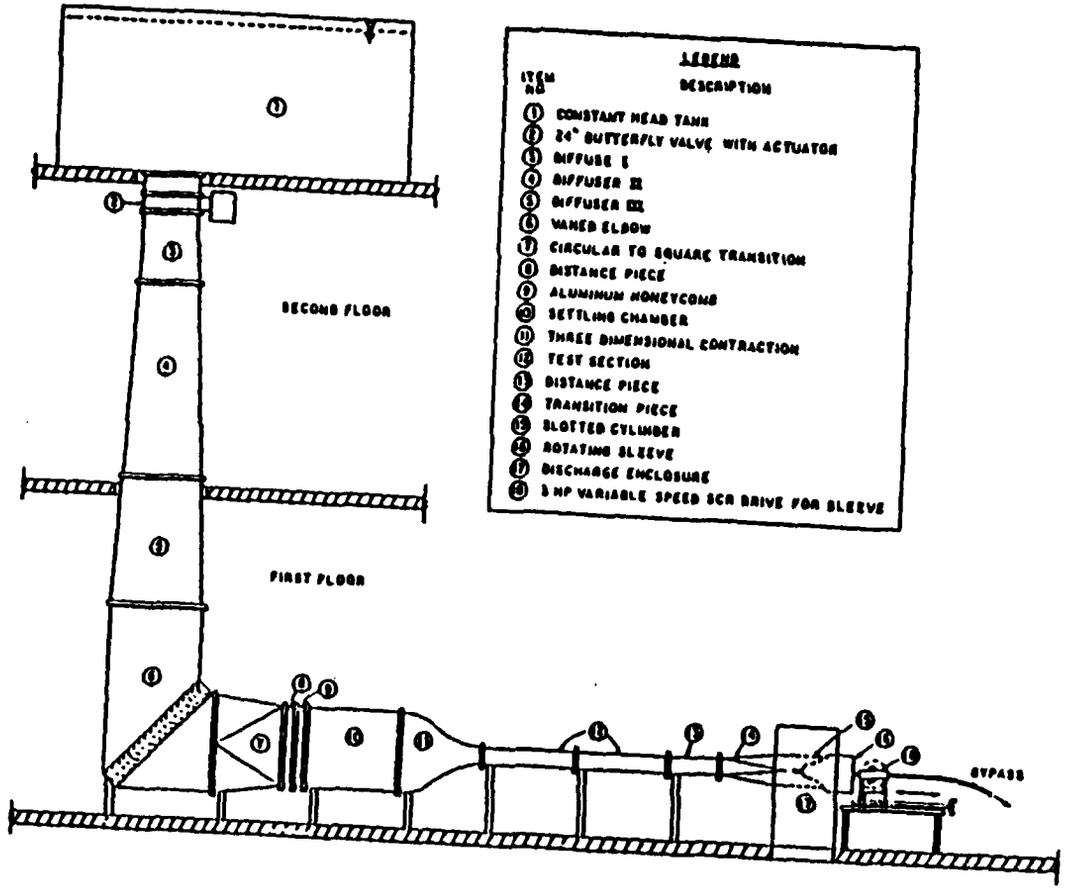

Figure 1 . Lay-out of the water tunnel.

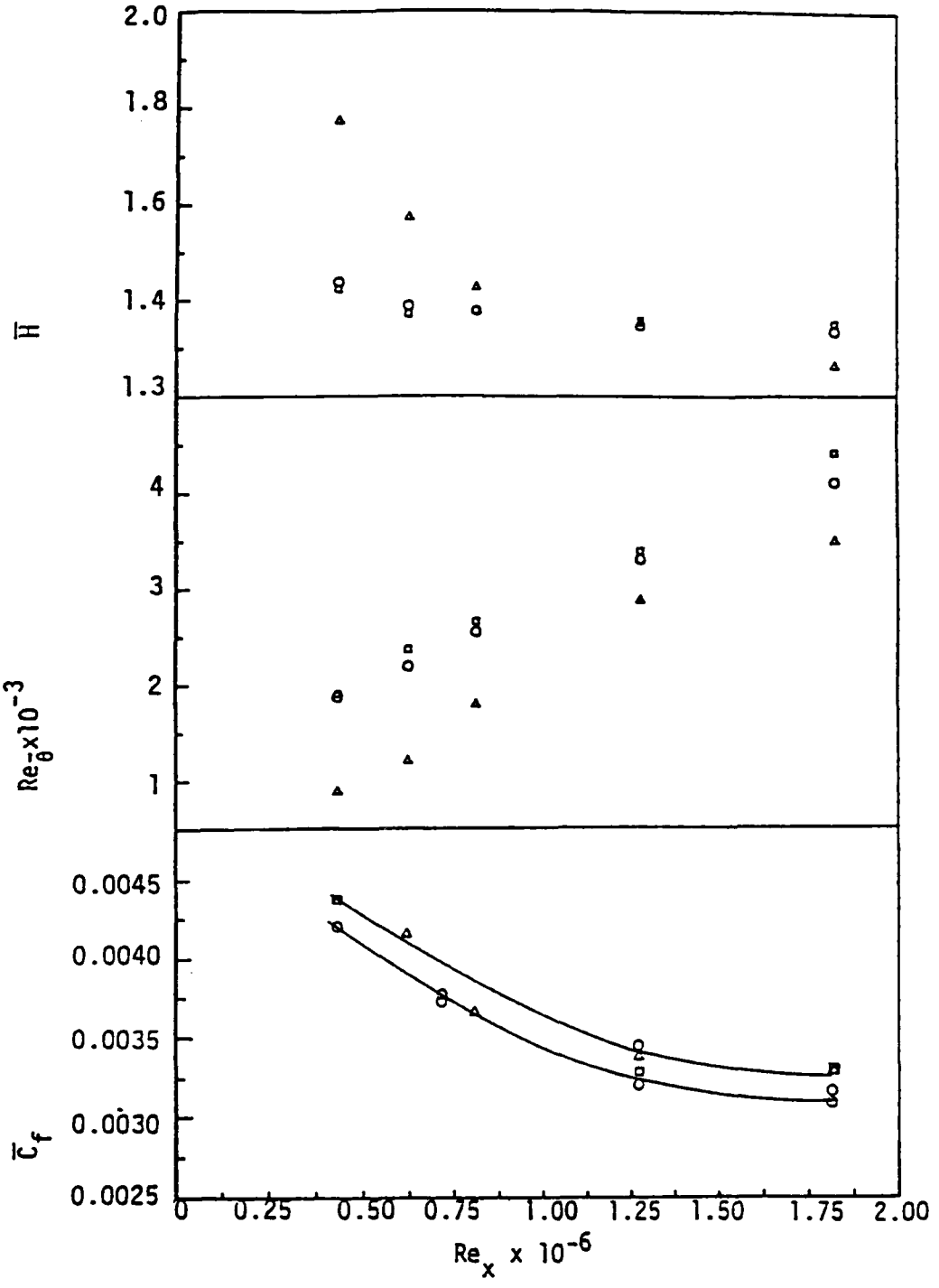

Figure 2. Longitudinal distribution of time-mean global properties of the boundary layer. Δ, steady flow; □, f = 0.5 Hz; O, f = 2Hz.

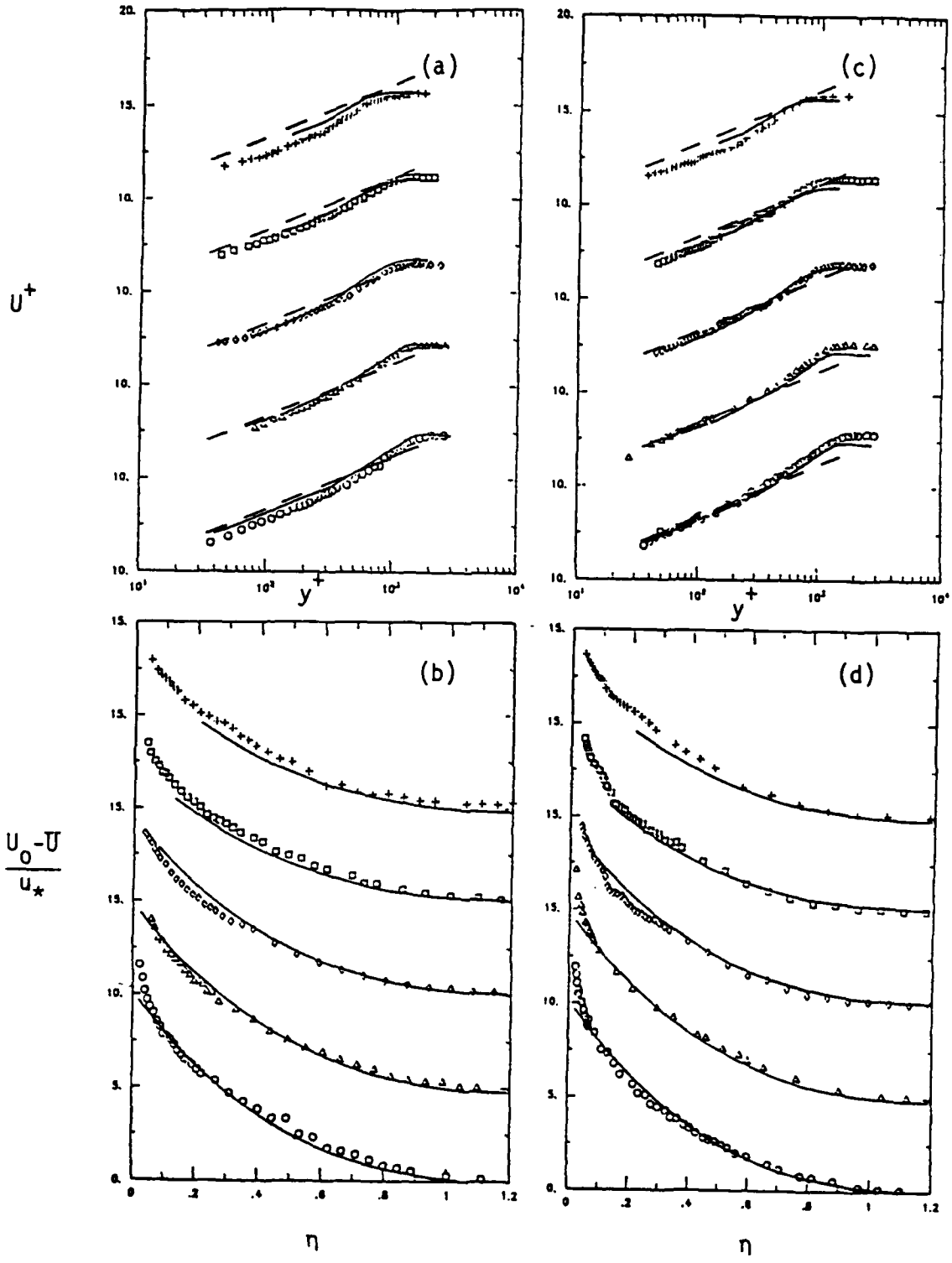

Figure 3. Mean velocity distributions in the boundary layer in the inner and outer coordinates. (a,b): 0.5Hz (c,d): 2Hz. Symbol, station: +,1; □,2; ◇,3; Δ,4; 0,5; ——, steady flow; ---,universal log law.

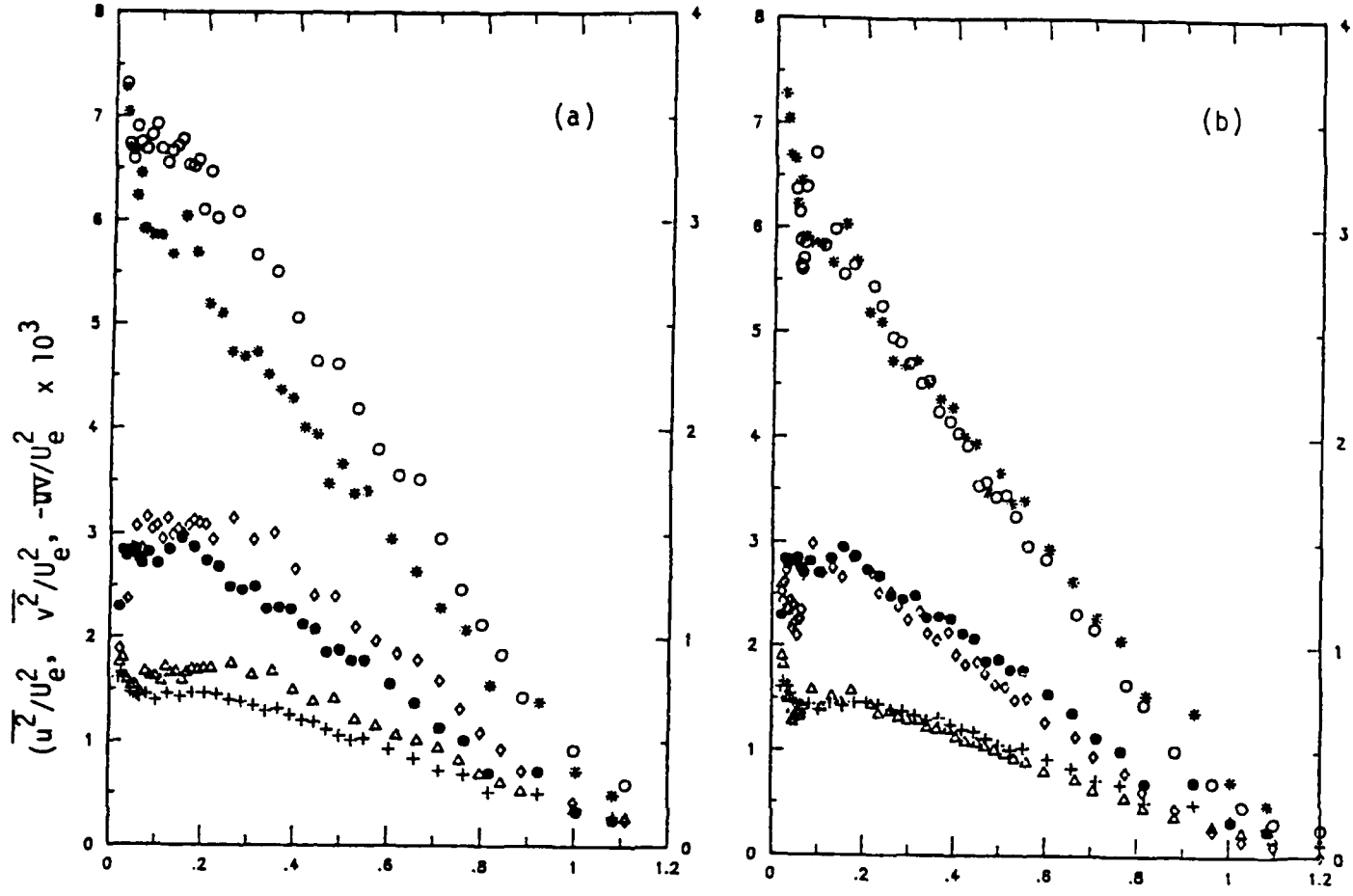

Figure 4. Distribution of $\overline{u^2}$, $\overline{v^2}$, and $-\overline{uv}$ at Station 5 (a) 0.5Hz (b) 2Hz {O, u^2; Δ, v^2; ◇, $-\overline{uv}$} (unsteady) {*, u^2; +, v^2; ●, $-\overline{uv}$} (steady).

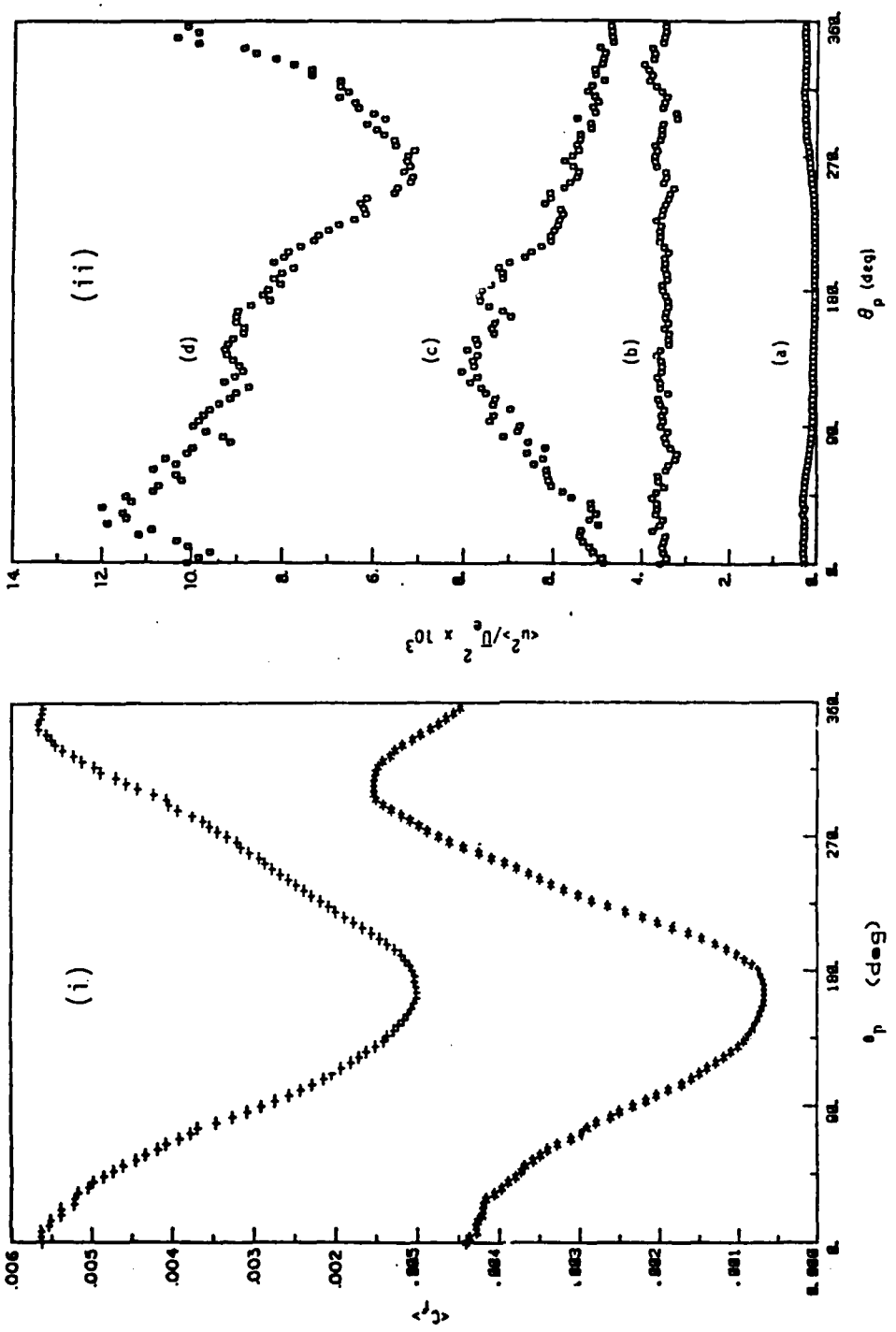

Figure 5. Variation of $\langle C_f \rangle$ and $\langle u^2 \rangle$ during the oscillation cycle, Station 5.
(i) $\langle C_f \rangle$: +, 0.5Hz; 0, 2Hz. (ii) $\langle u^2 \rangle$ (at 2Hz): (a) $\eta = 1.80$,
(b) $\eta = 0.47$, (c) $\eta = 0.068$, (d) $\eta = 0.023$.

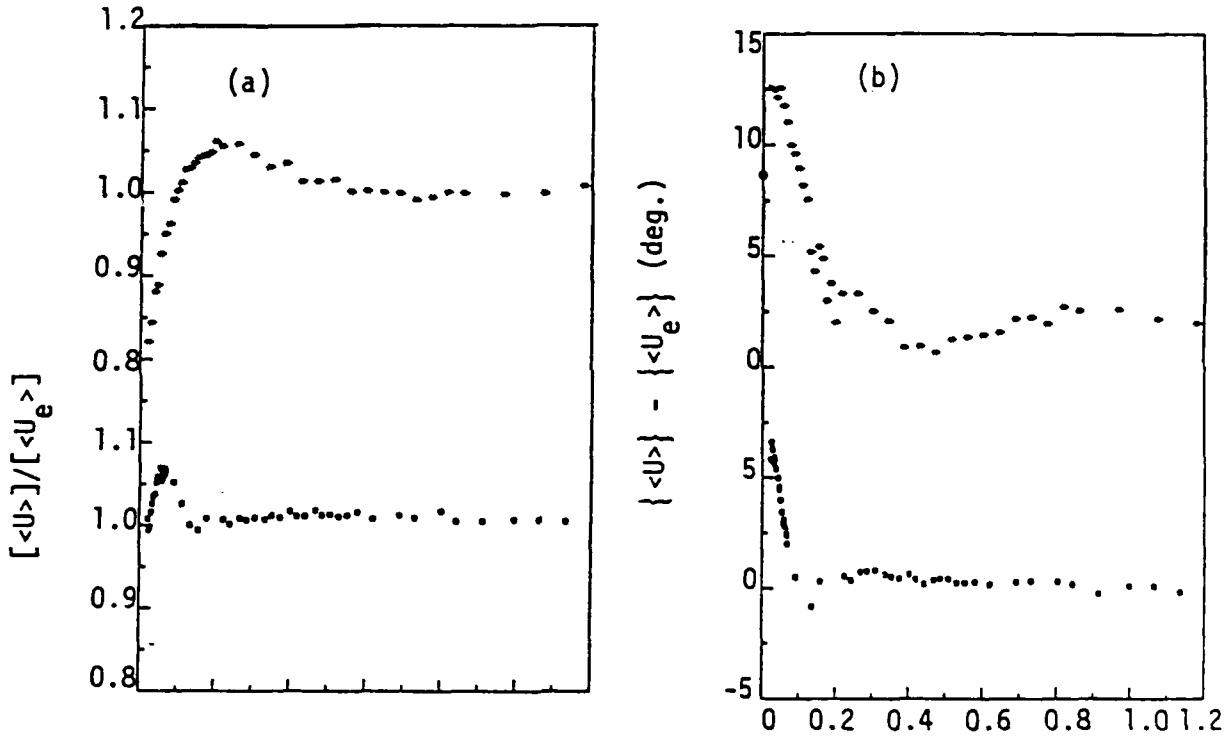

Figure 6. Behavior of the oscillatory component of <U> at station 5. (a) amplitude (b) phase *, 0.5Hz; □, 2Hz. Note [ ] denotes amplitude and { } denotes phase.

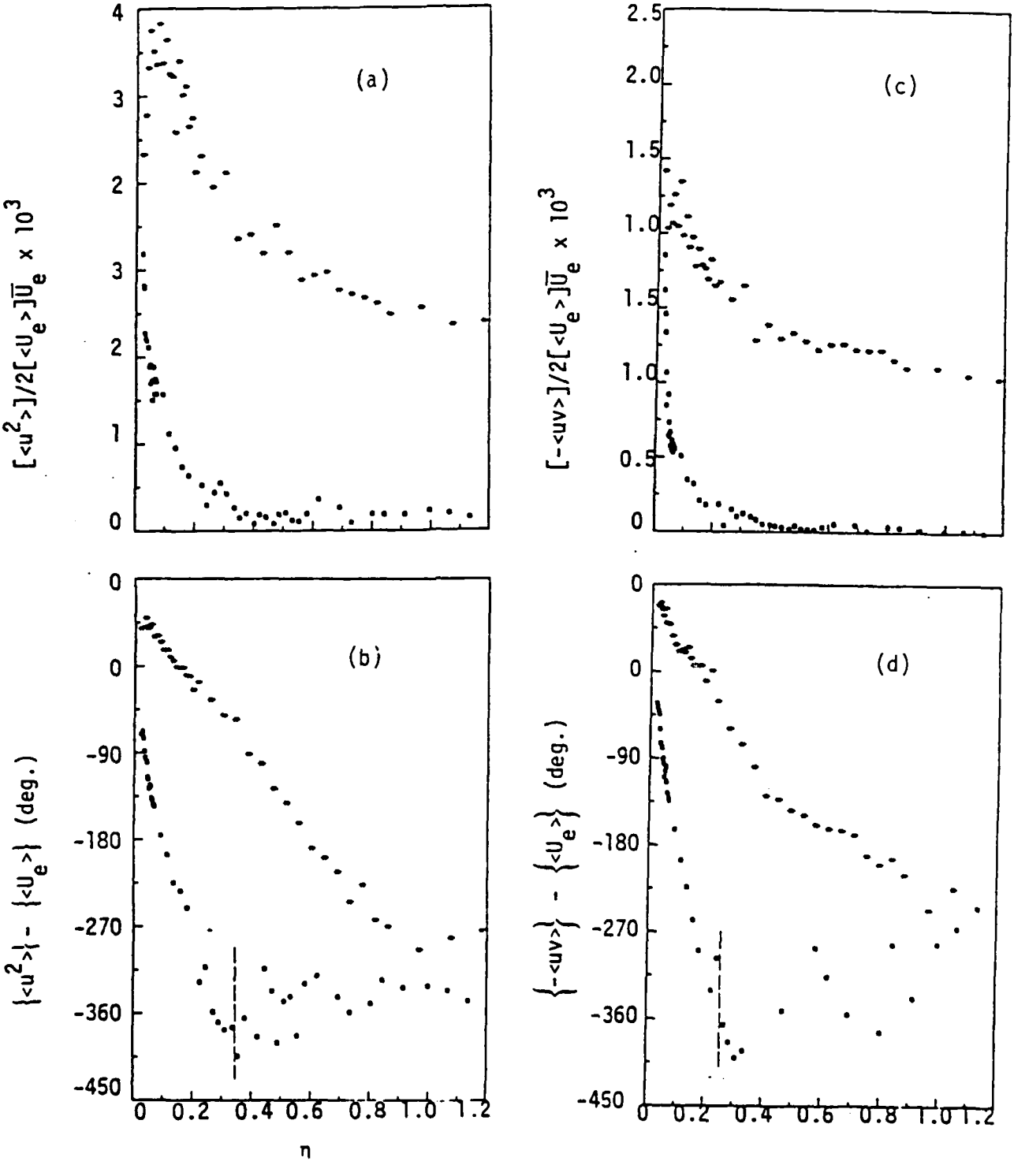

Figure 7. Behavior of the oscillatory component of $<u^2>$ and $<-uv>$ (a) amplitude of $<u^2>$ (b) phase of $<u^2>$ (c) amplitude of $<-uv>$ (d) phase of $<-uv>$. *, 0.5Hz; □, 2Hz.

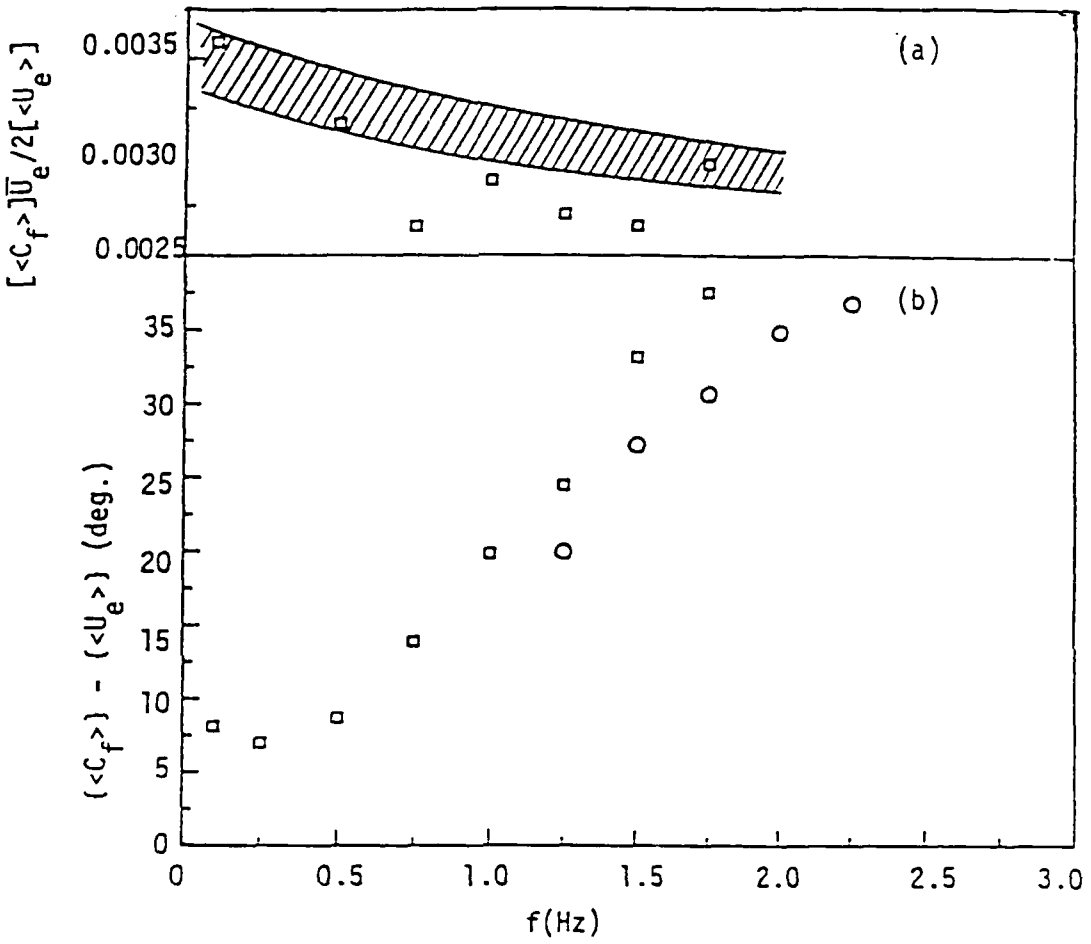

Figure 8. Frequency dependence of wall shear stress at Station 5. (a) amplitude (b) phase. □, using sleeve designed for 0.5Hz; 0, using sleeve designed for 2.0Hz; ////, Time-mean value $\overline{C}_f$.

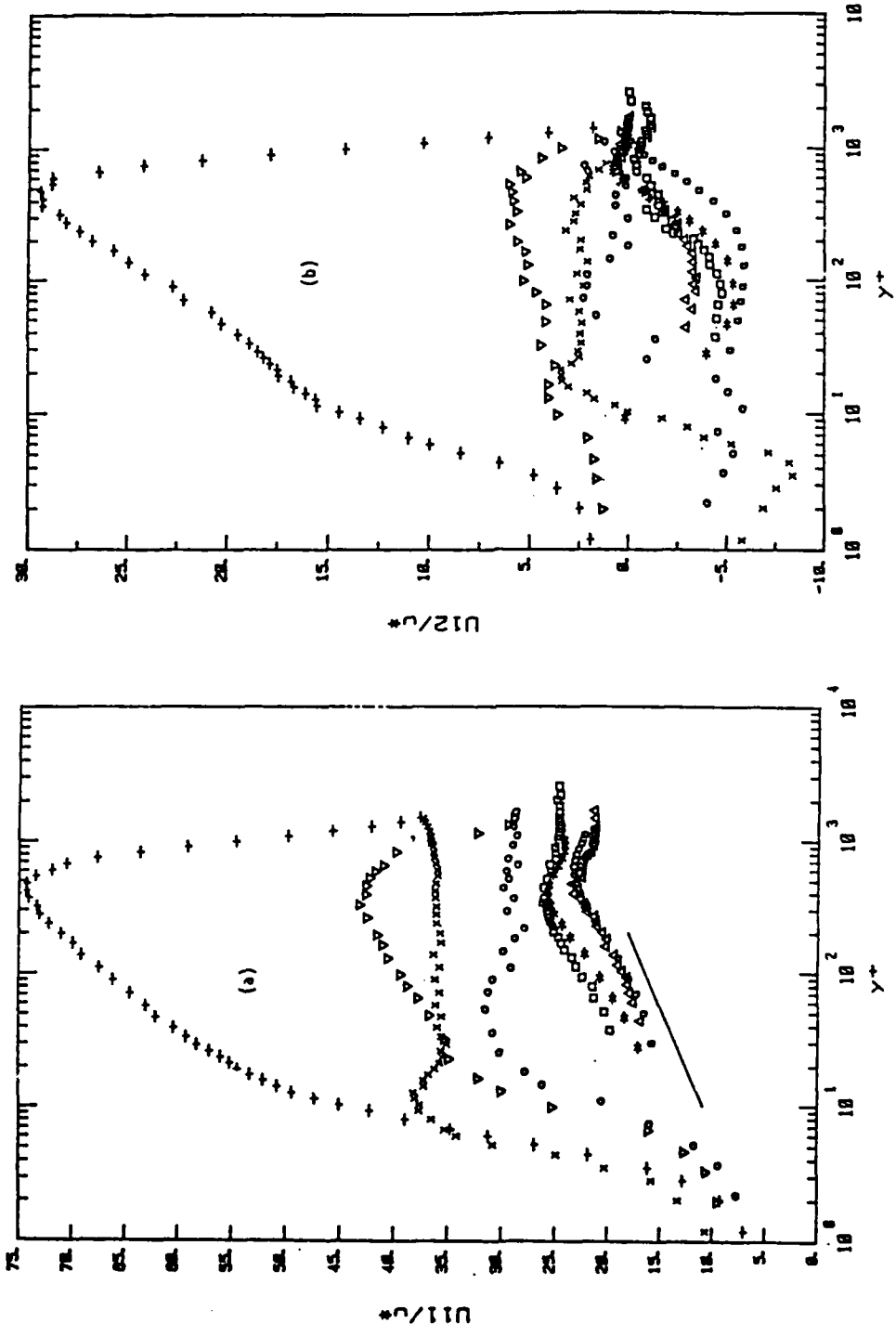

Figure 9. Oscillatory velocity components in the inner coordinates (a) in-phase component (b) out-of-phase component. Δ, experiment M1; □, M5; *, CA; O, T1; ▽,J1; o,J2; +,J3; x,J4; -,universal logarithmic law.

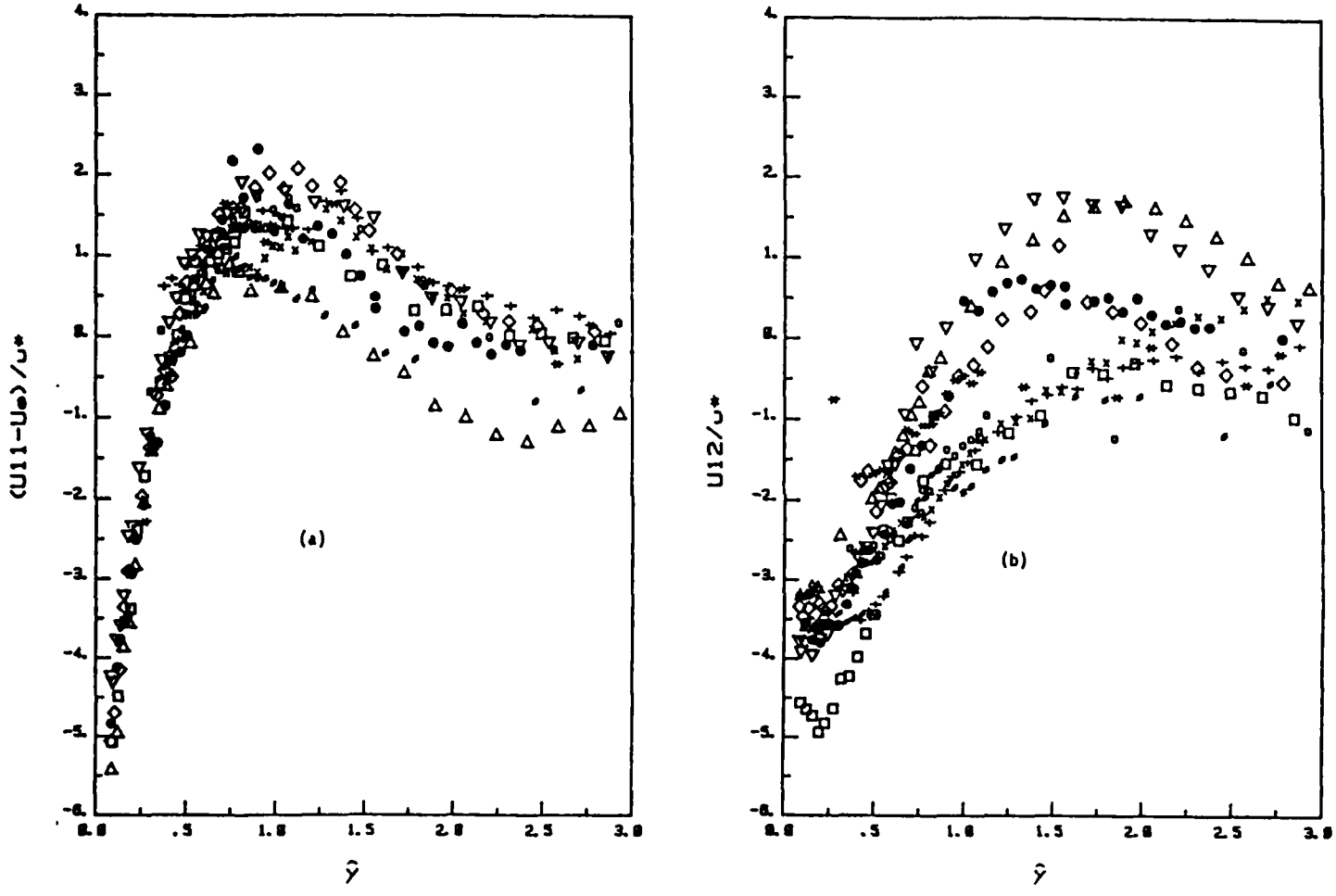

Figure 10. Oscillatory velocity components in the unsteady vortical layer coordinates. Present experimental results (a) in-phase component, (b) out-of-phase compomnent. ●, experiment M1; ◇, M2; ▽, M3; △, M4; □, M5; #, M6; X, M7; +, M8; *, M9; 0, M10.

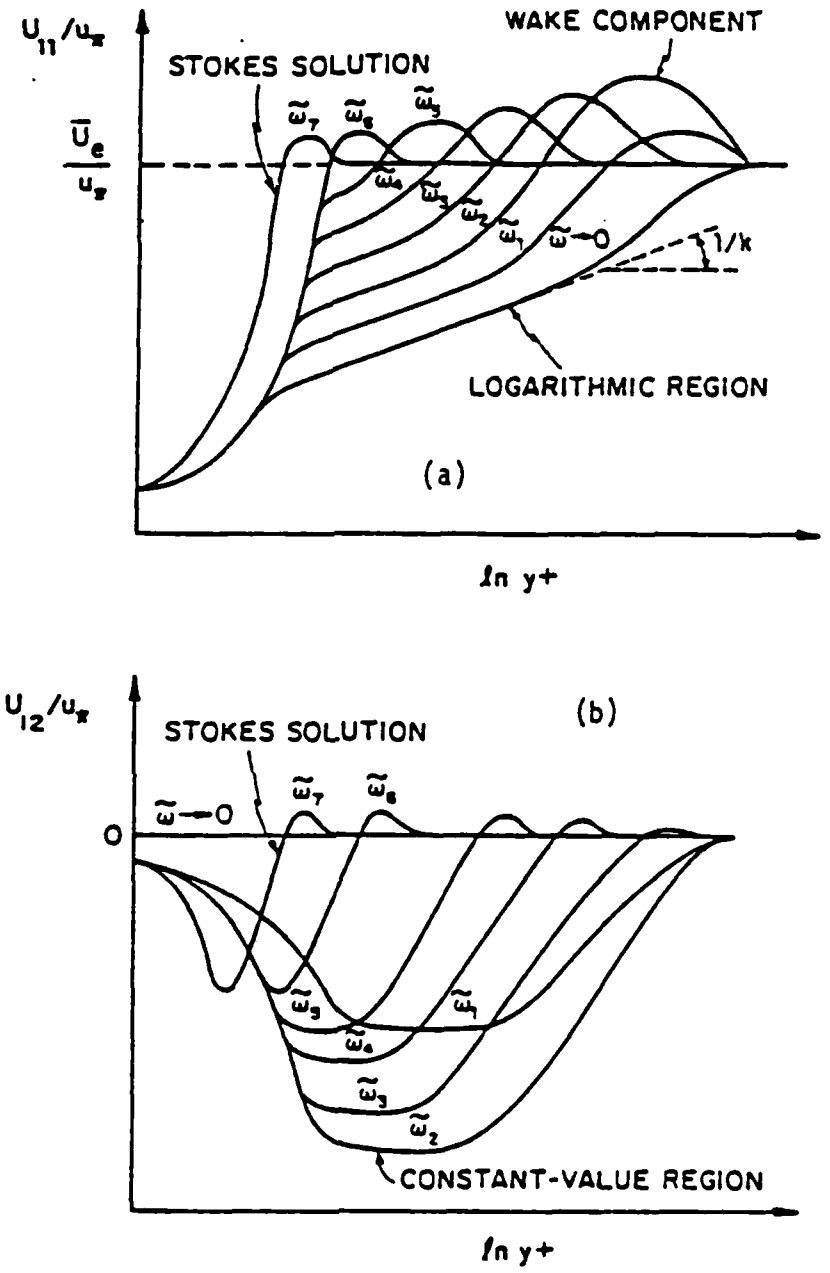

Figure 11. Qualitative representation of the evolution of the in-phase and out-of-phase velocity components with $\tilde{\omega}$. $0 < \tilde{\omega}_1 < \tilde{\omega}_2 < \ldots < \tilde{\omega}_7$. (a) In-phase component. (b) Out-of-phase component.

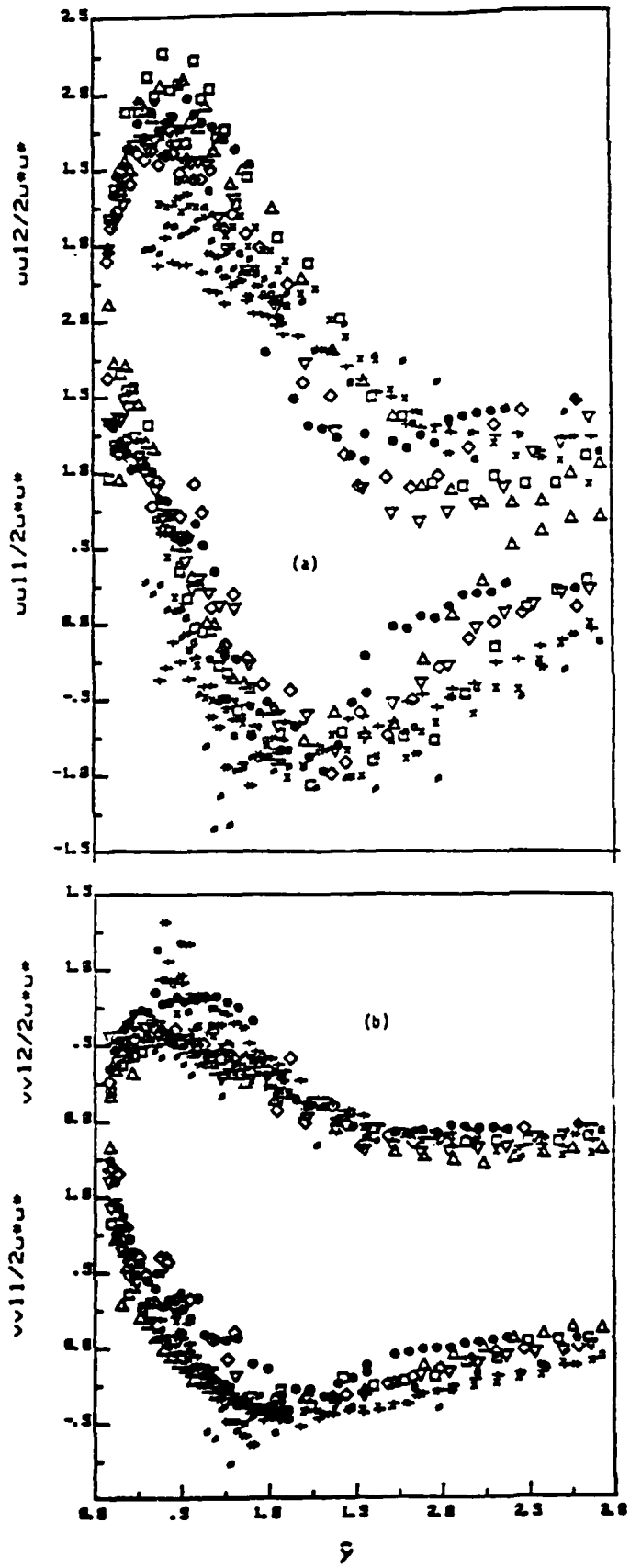

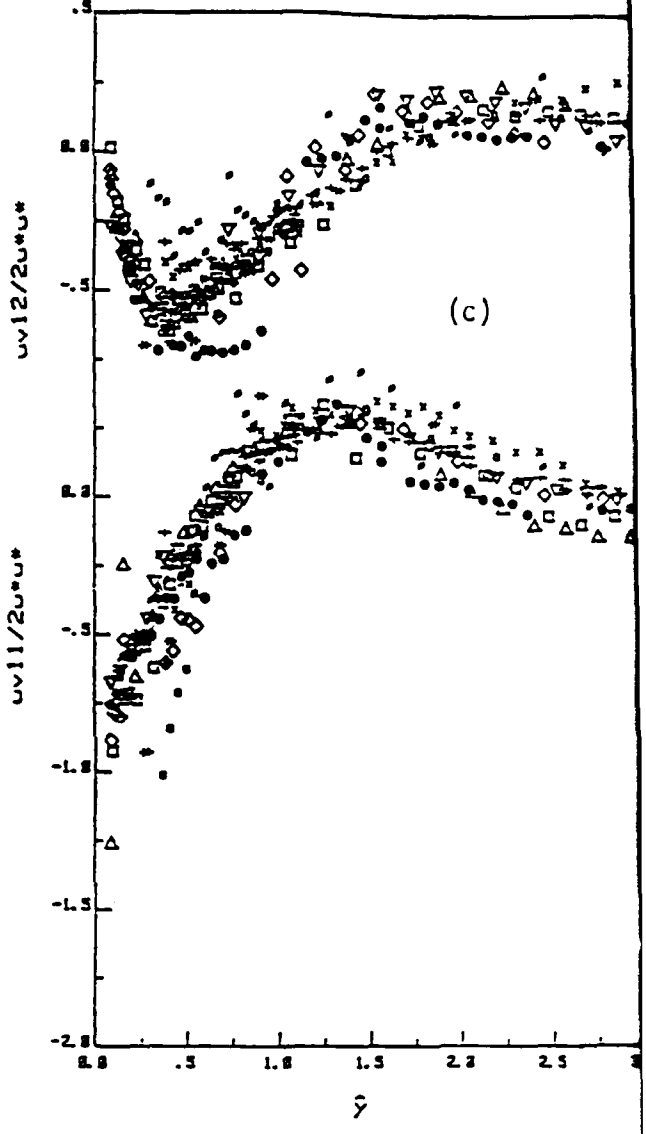

Figure 12. Oscillatory components of $\langle u^2 \rangle$ $\langle v^2 \rangle$ and $-\langle uv \rangle$ in unsteady vortical layer coordinates. Symbol as in figure 11. Subscript 11 denotes in-phase, subscript 22 denotes out-of-phase.

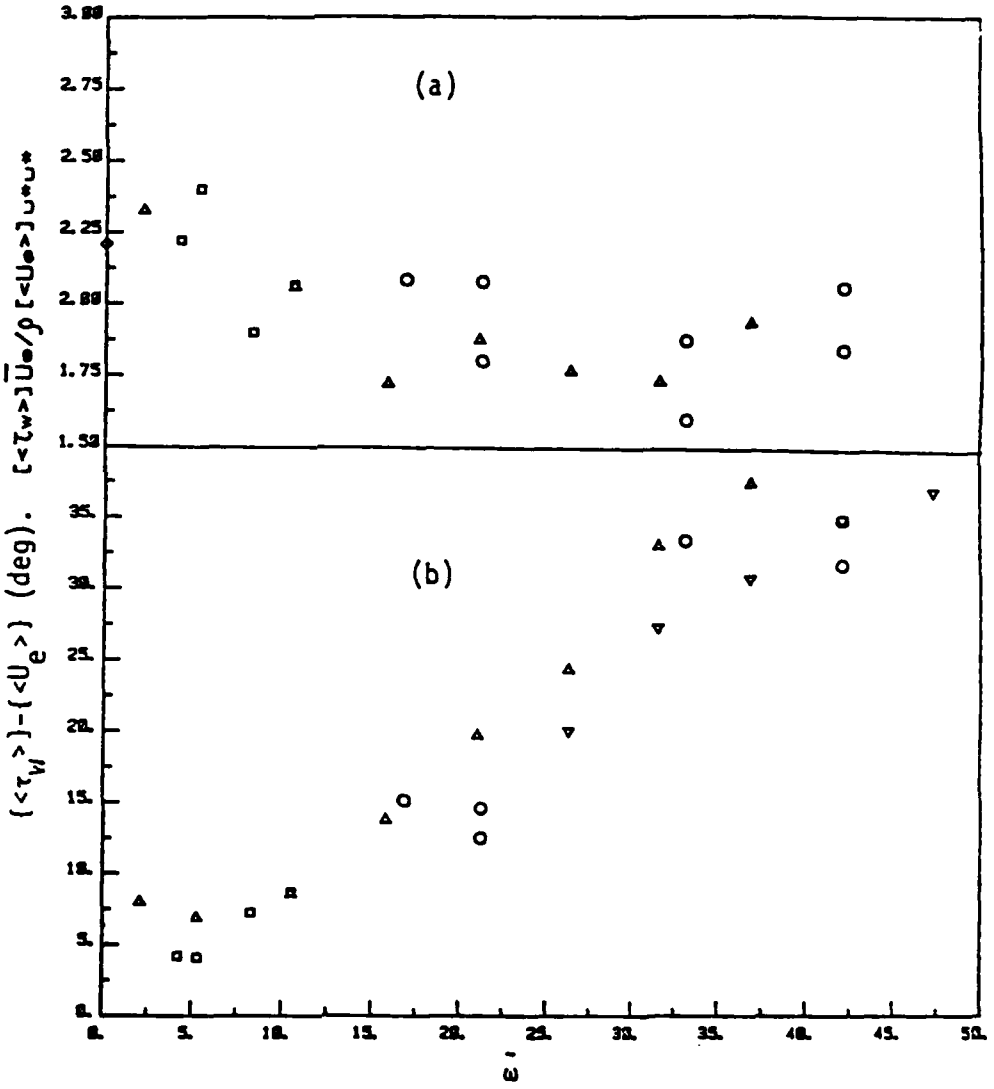

Figure 13. Correlation of the oscillatory wall shear stress in terms of $\bar{\omega}$. (a) Amplitude. (b) Phase. □, f = 0.5 Hz, ○, f = 2 Hz; △, station 5, 0.5 Hz sleeve; ▽, station 5, 2 Hz sleeve; ◇, quasi-steady value.

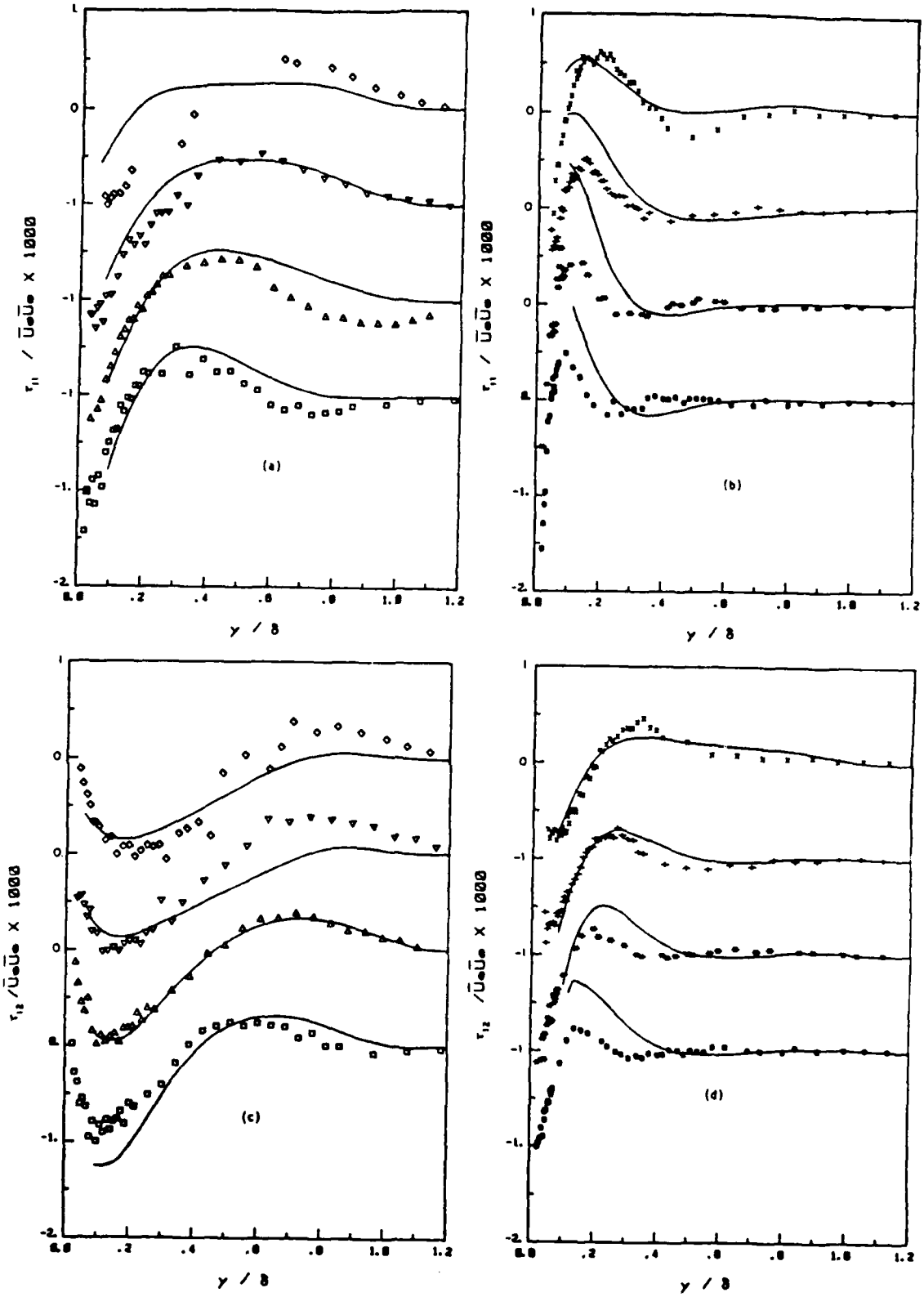

Fig.14. Comparison of predictions with ZPG experimental data of amplitude and phase of velocity. a, c: 0.5 Hz; b, d: 2.0 Hz. —, predictions; symbol, stations: □, 2; △, 3;▽, 4;◇, 5. The initial conditions were matched at station 1.

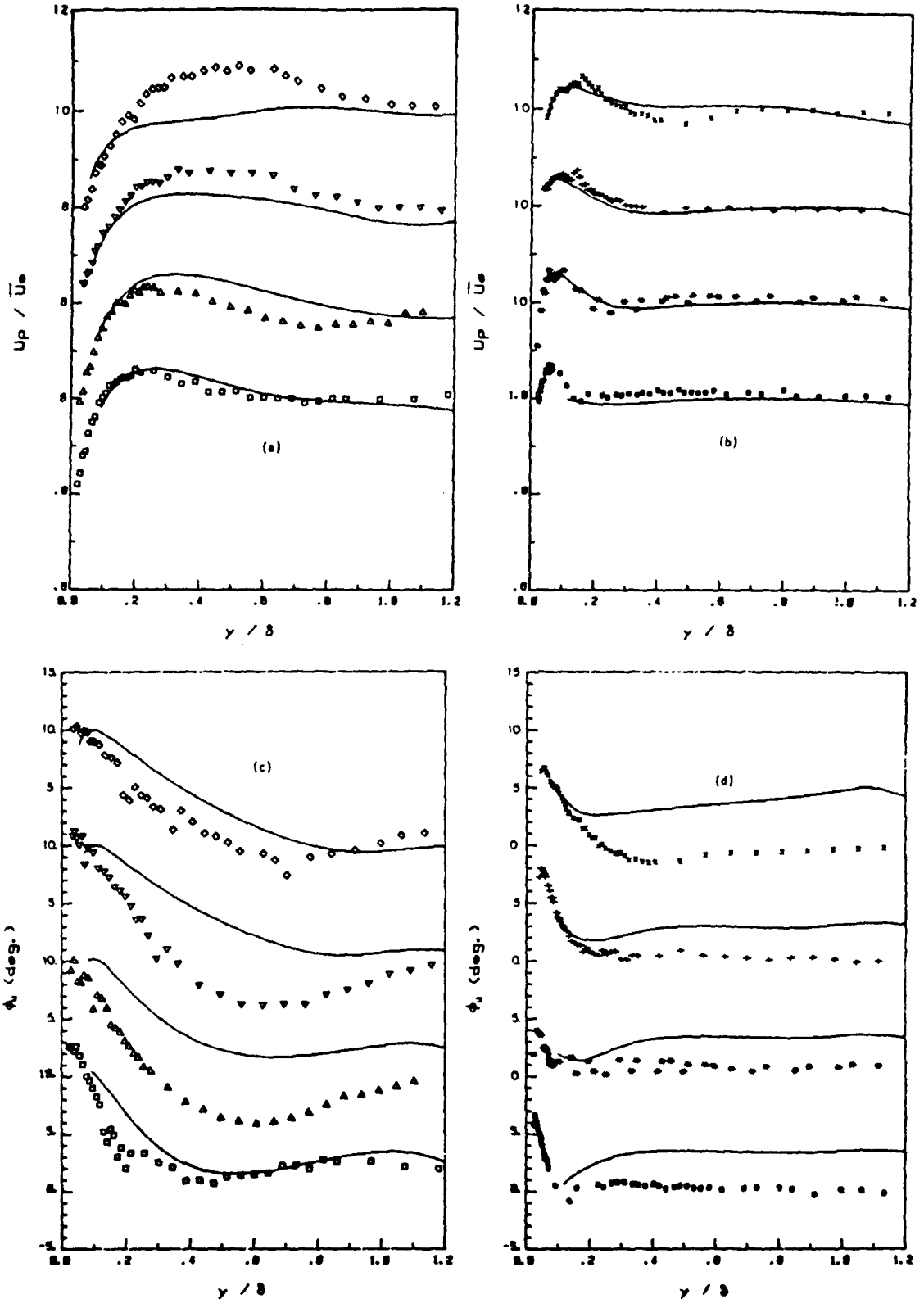

Fig.15. Comparison of predictions with ZPG experimental data of in-phase and out-of-phase components of Reynolds shear stress. a, c: 0.5 Hz; b, d: 2.0 Hz. symbols as in figure 14.

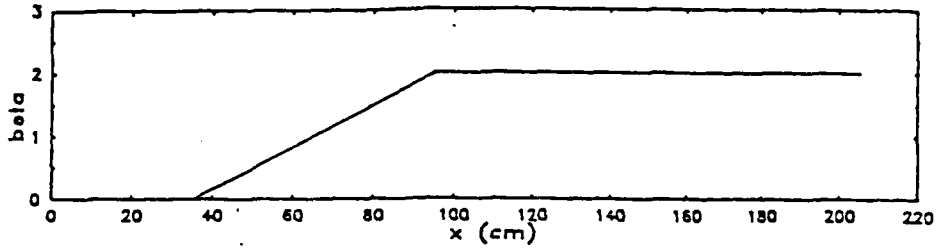

Fig.16. Imposed distribution of Clauser parameter β along the test section for the case of mild adverse pressure gradient.

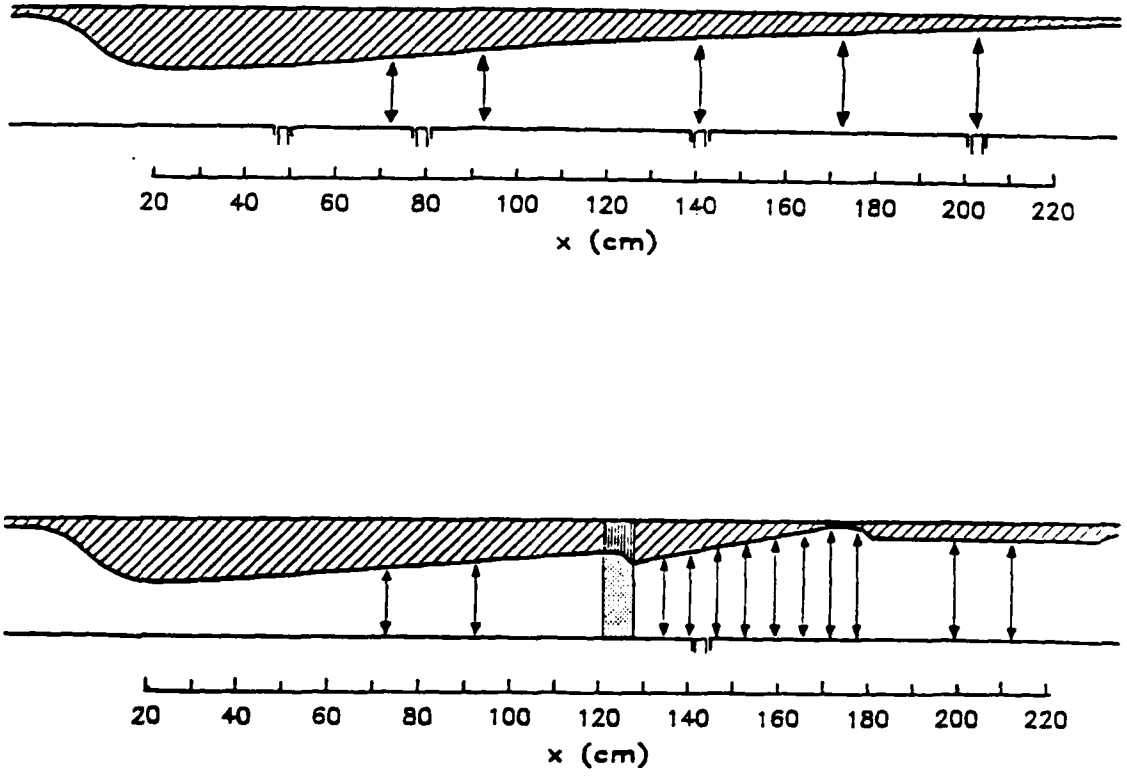

Fig.17. Top wall geometries for mild and strong pressure gradients. The velocity measurement stations are indicated by the arrows. The locations of HFG are marked on the lower wall. For the strong adverse pressure gradient, the section, where boundary layer suction was introduced is shown.

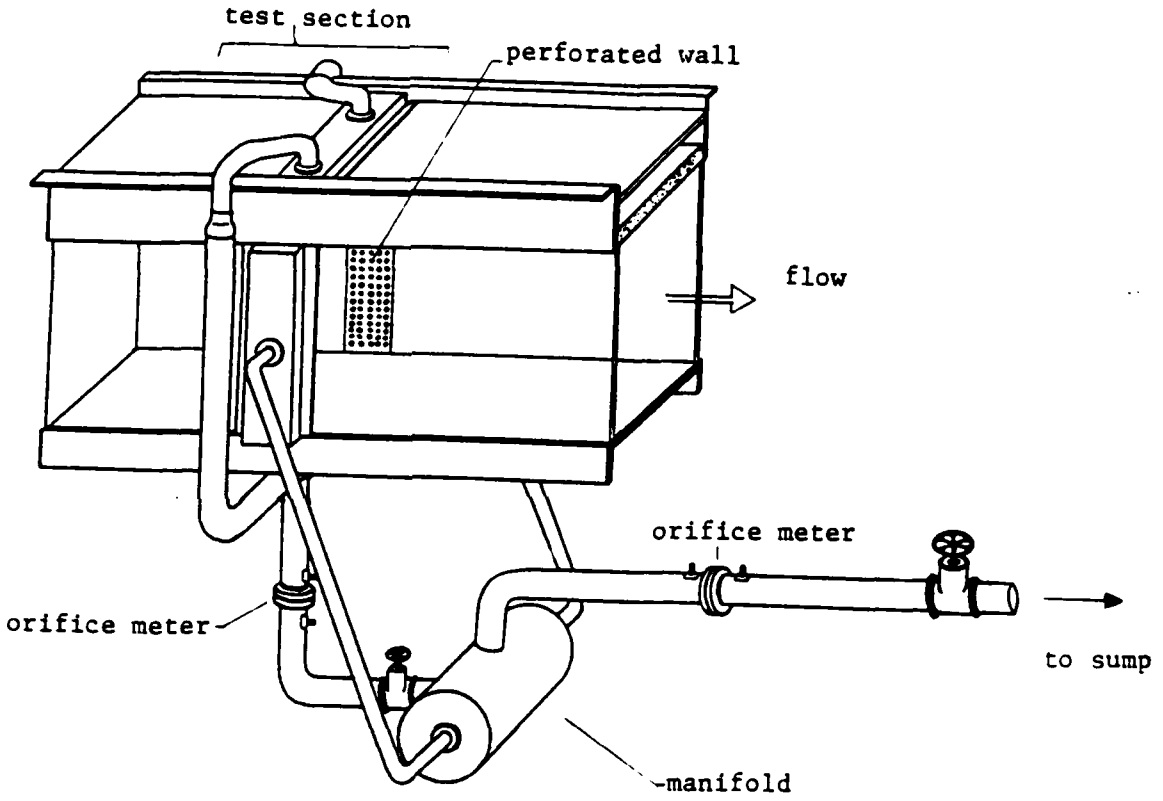

Fig.18. Details of the suction arrangement for the control of the boundary layer.

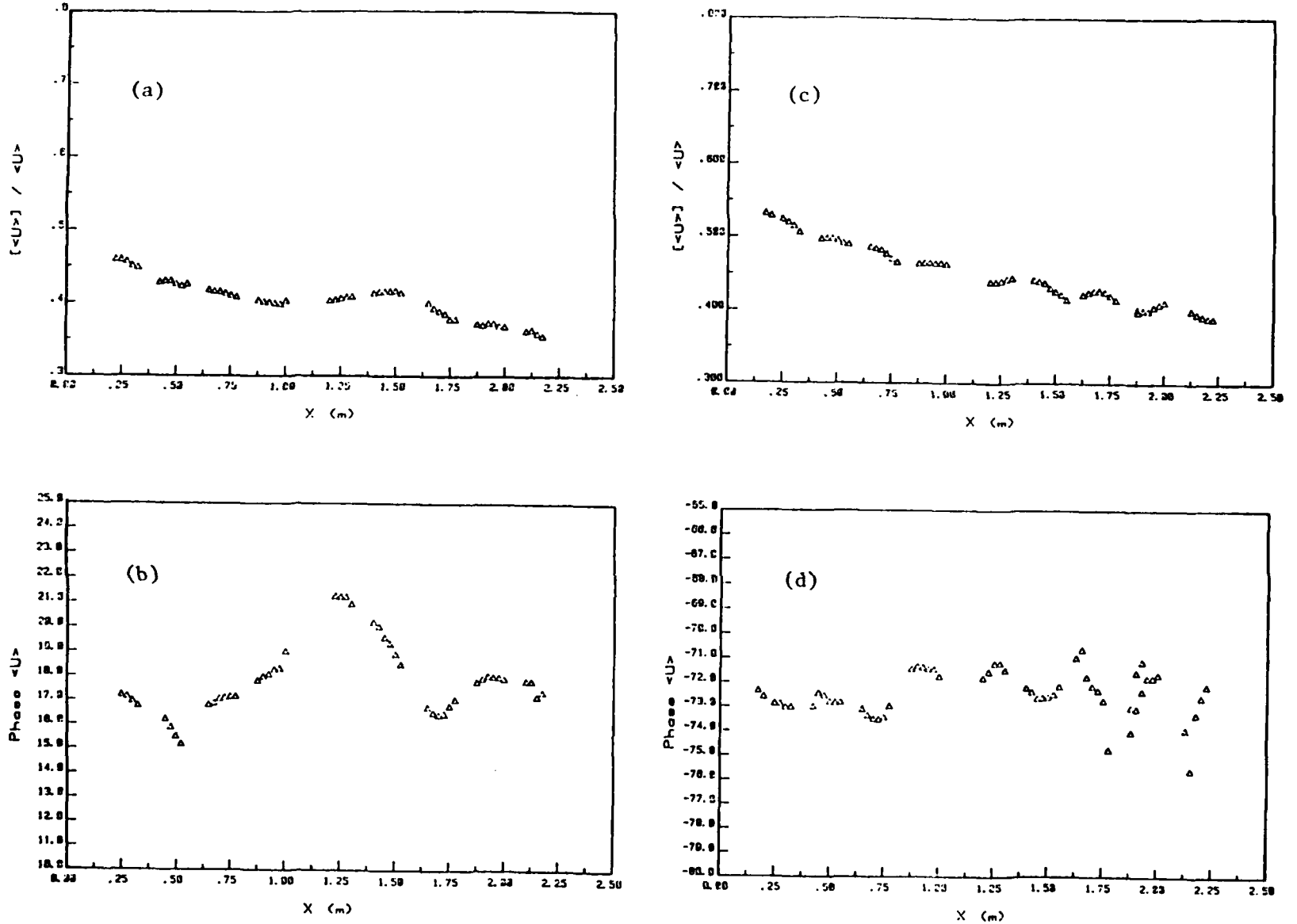

Fig.19. Longitudinal profiles of amplitude and phase of the freestream velocity. a, b: 0.5 Hz; c, d: 2.0 Hz.

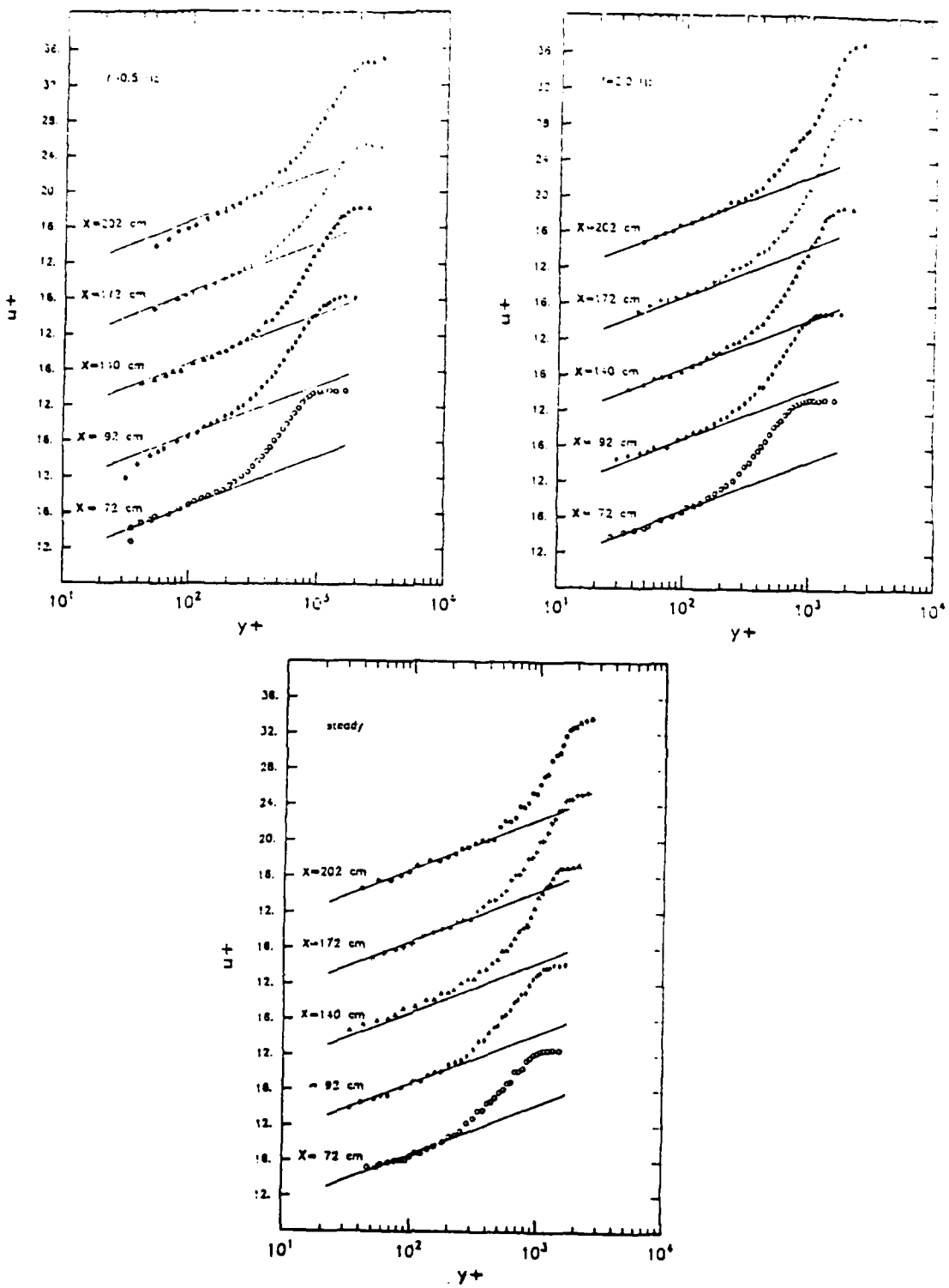

Fig.20. Time-mean velocity distributions in mild adverse pressure gradient. —, universal logarithmic law.

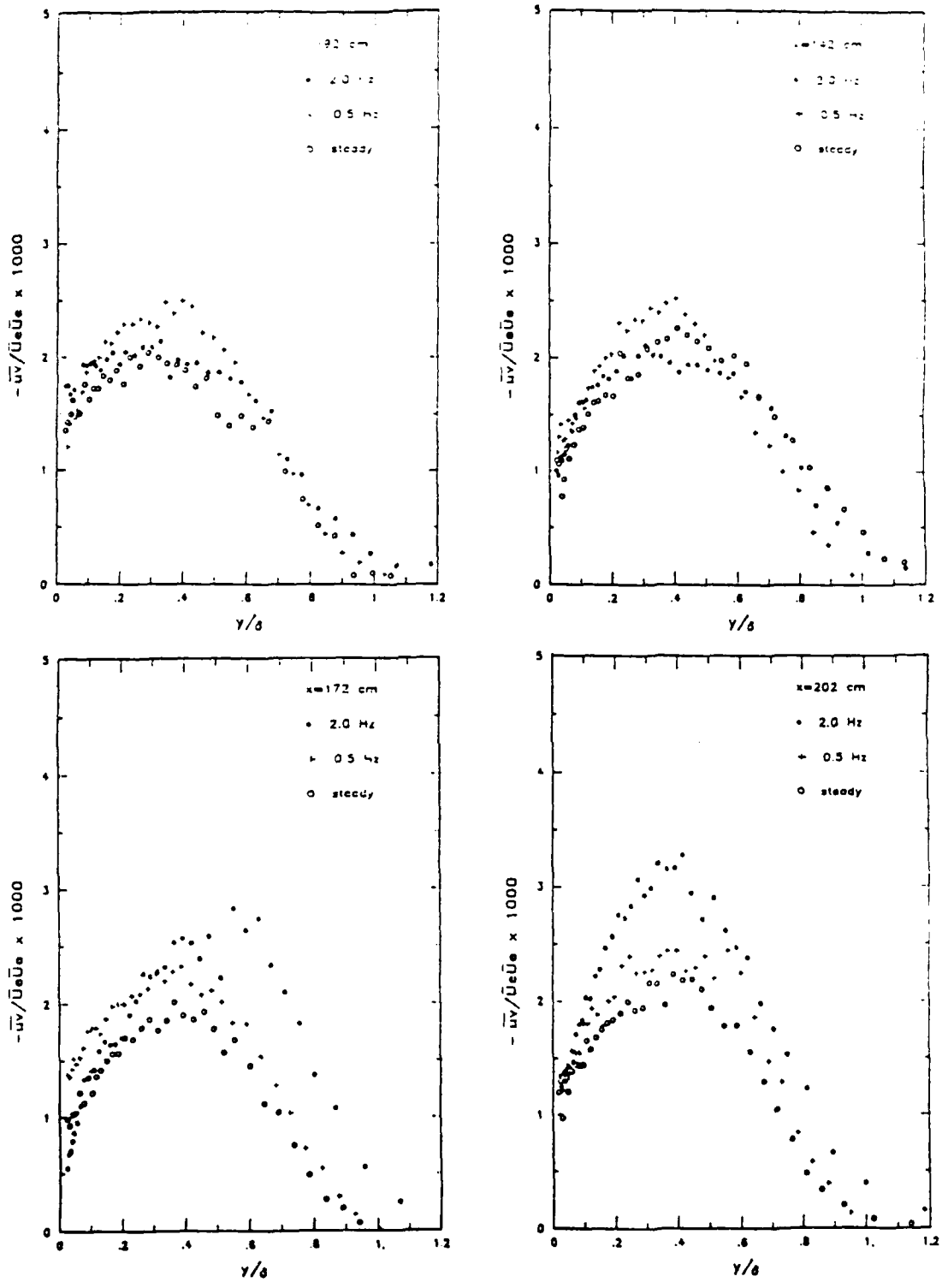

Fig.21. Long-time averaged Reynolds shear stresses in mild adverse pressure gradient.

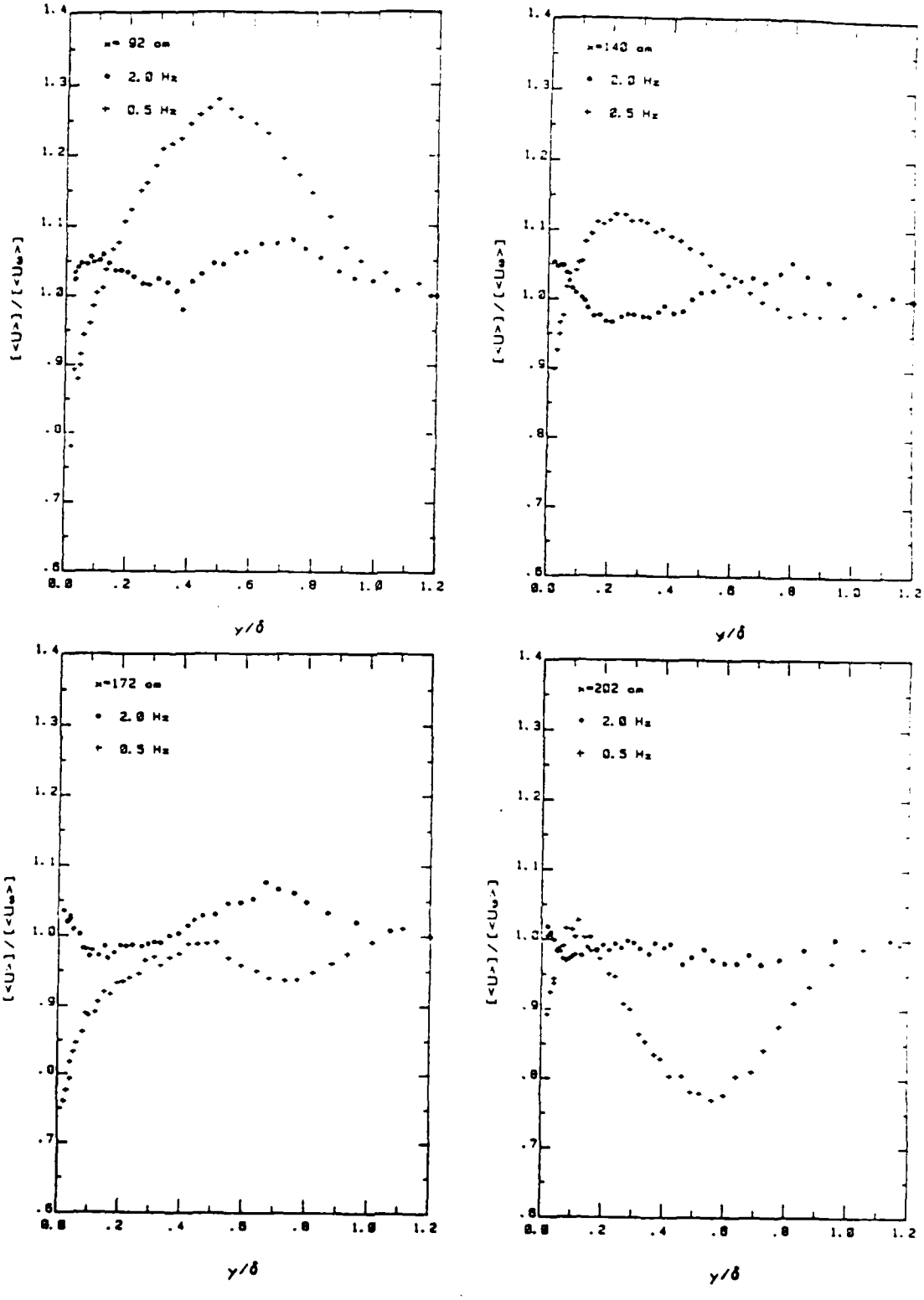

Fig.22. Distributions of the amplitude of the oscillatory velocity in mild adverse pressure gradient.

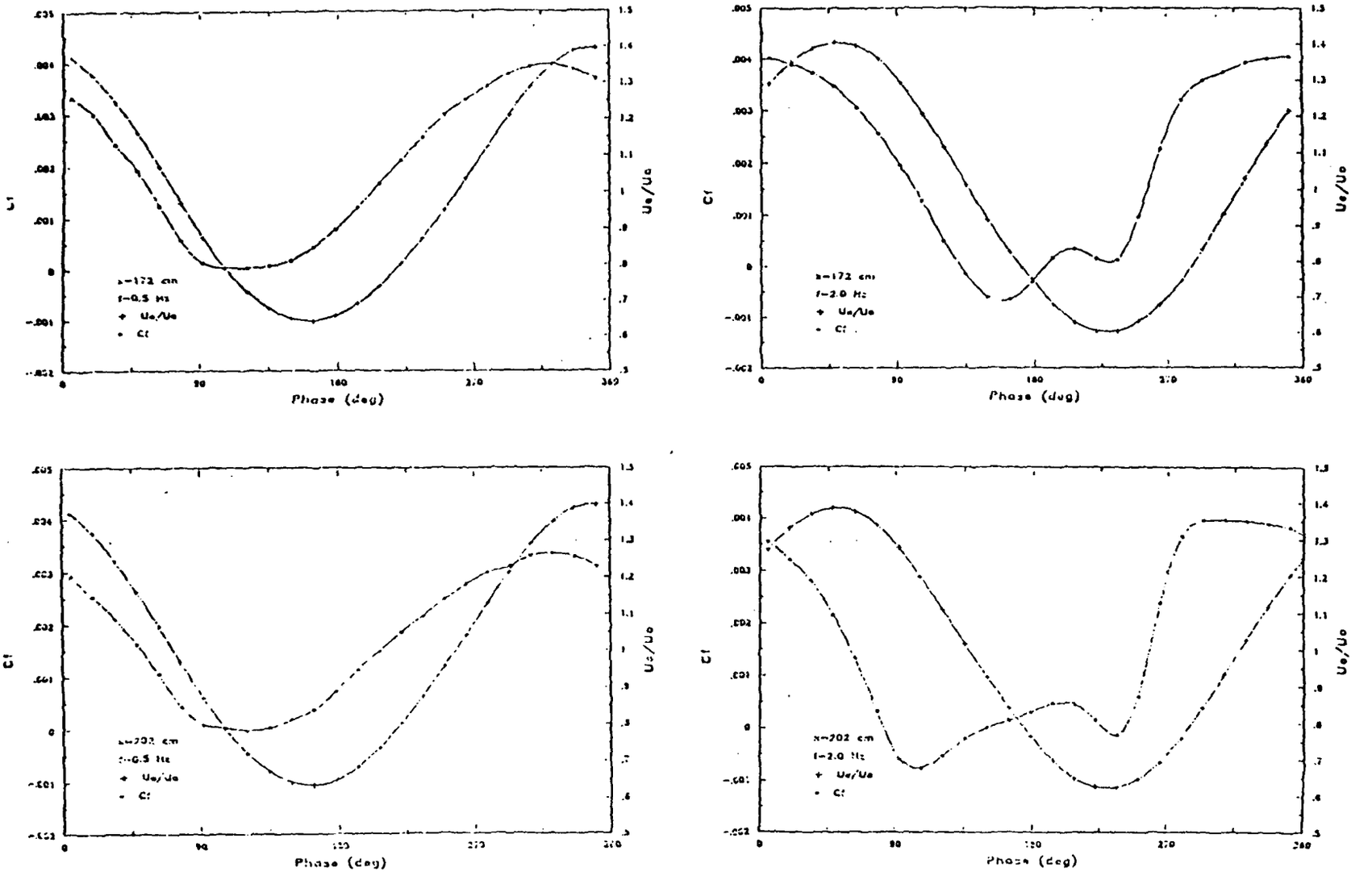

Fig.23. Variation of $\langle C_f \rangle$ during the oscillatory cycle in mild adverse pressure gradient.

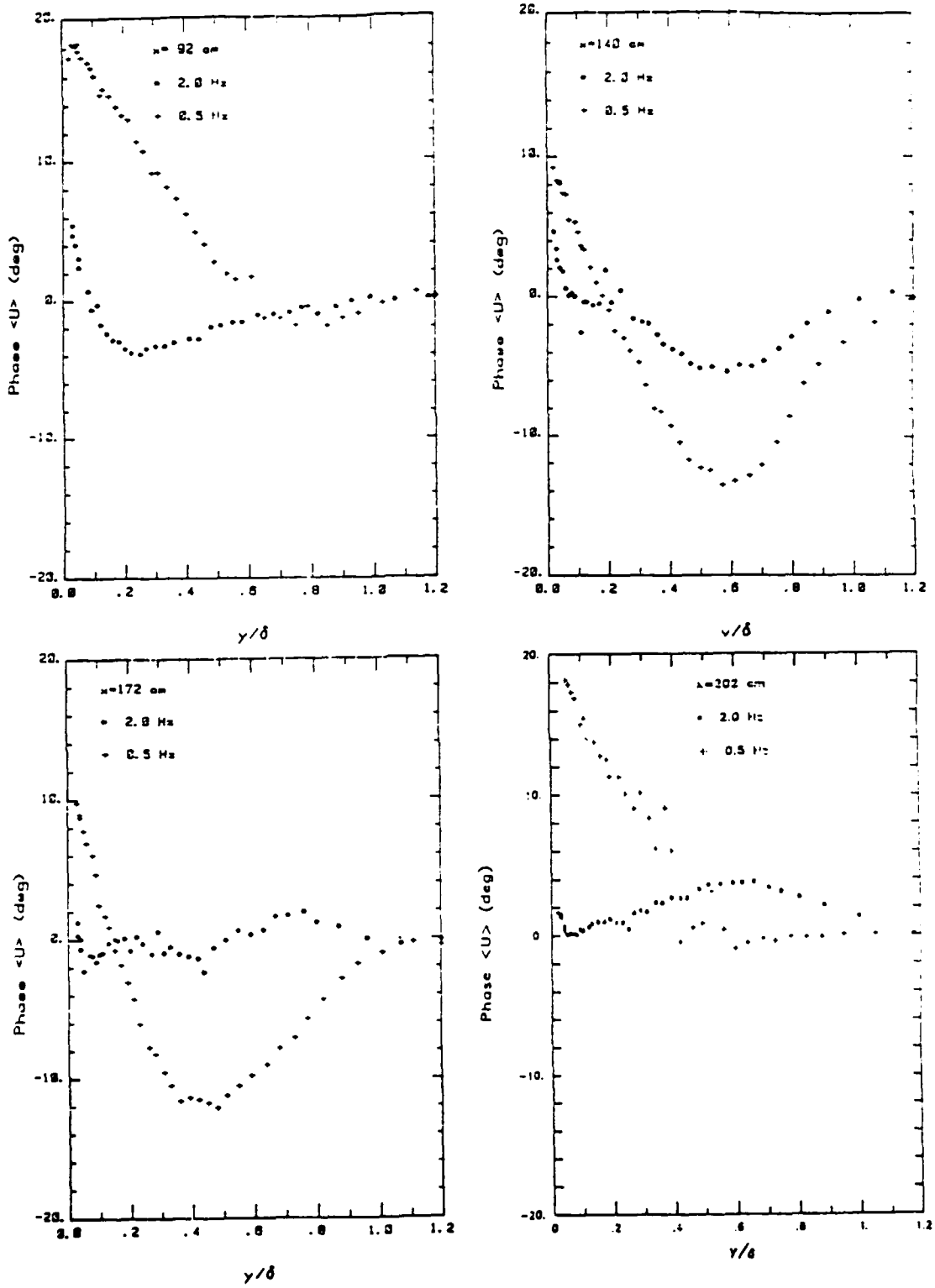

Fig.24. Distributions of the phase of the oscillatory velocity in mild adverse pressure gradient.

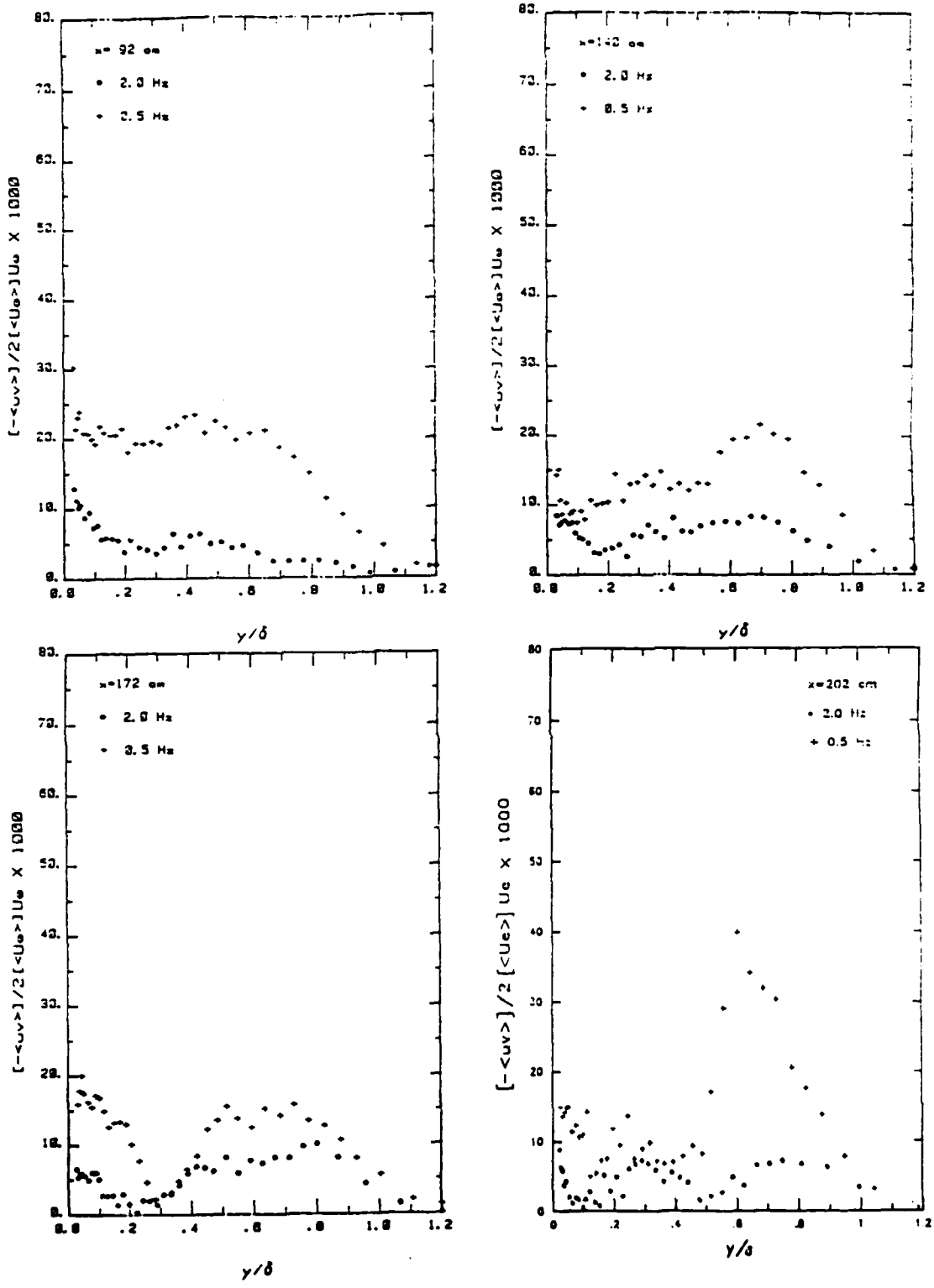

Fig.25. Distributions of the amplitude of $\langle -uv \rangle$ in mild adverse pressure gradient.

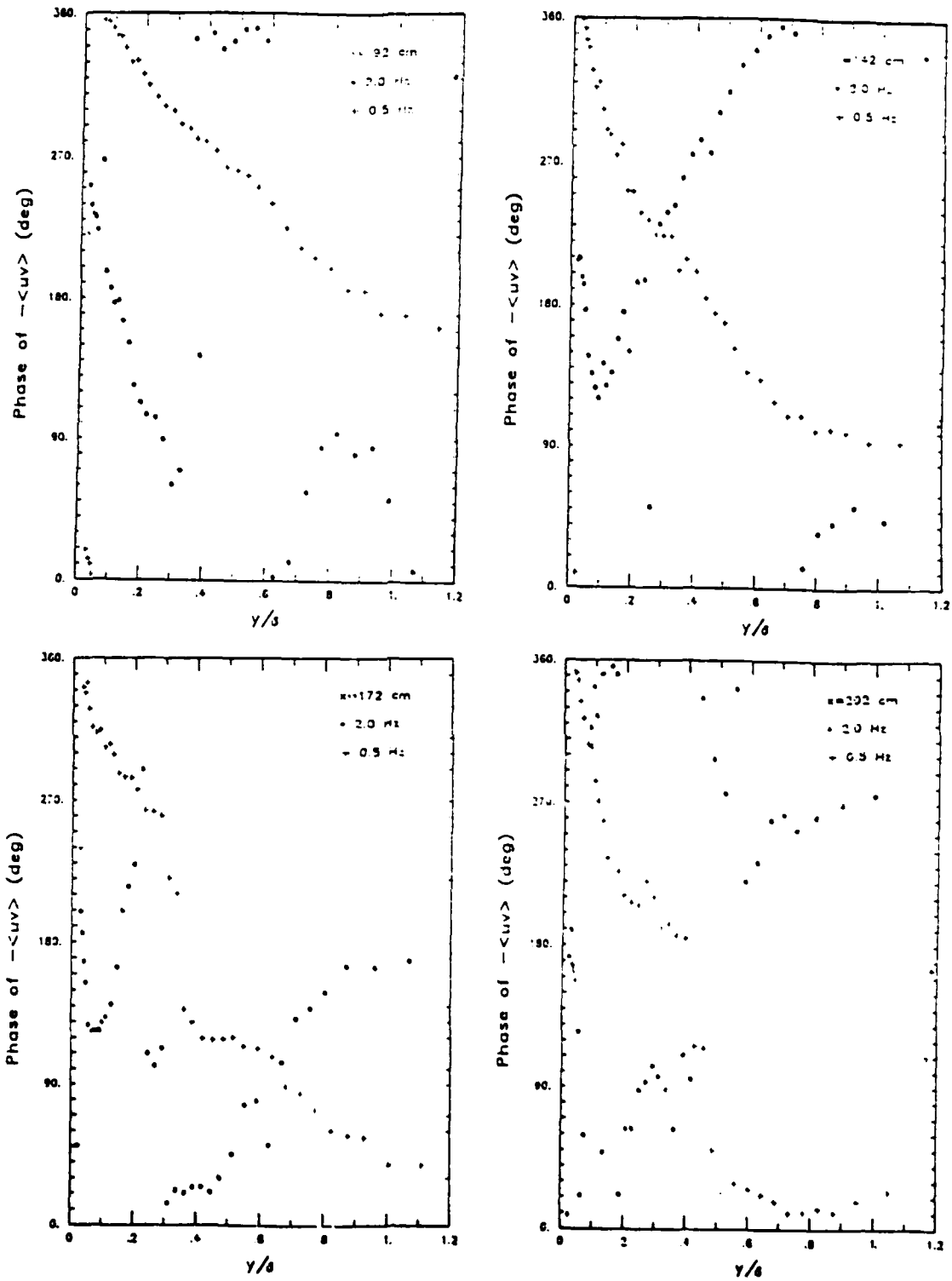

Fig.26. Distributions of the phase of $(-uv)$ in mild adverse pressure gradient.

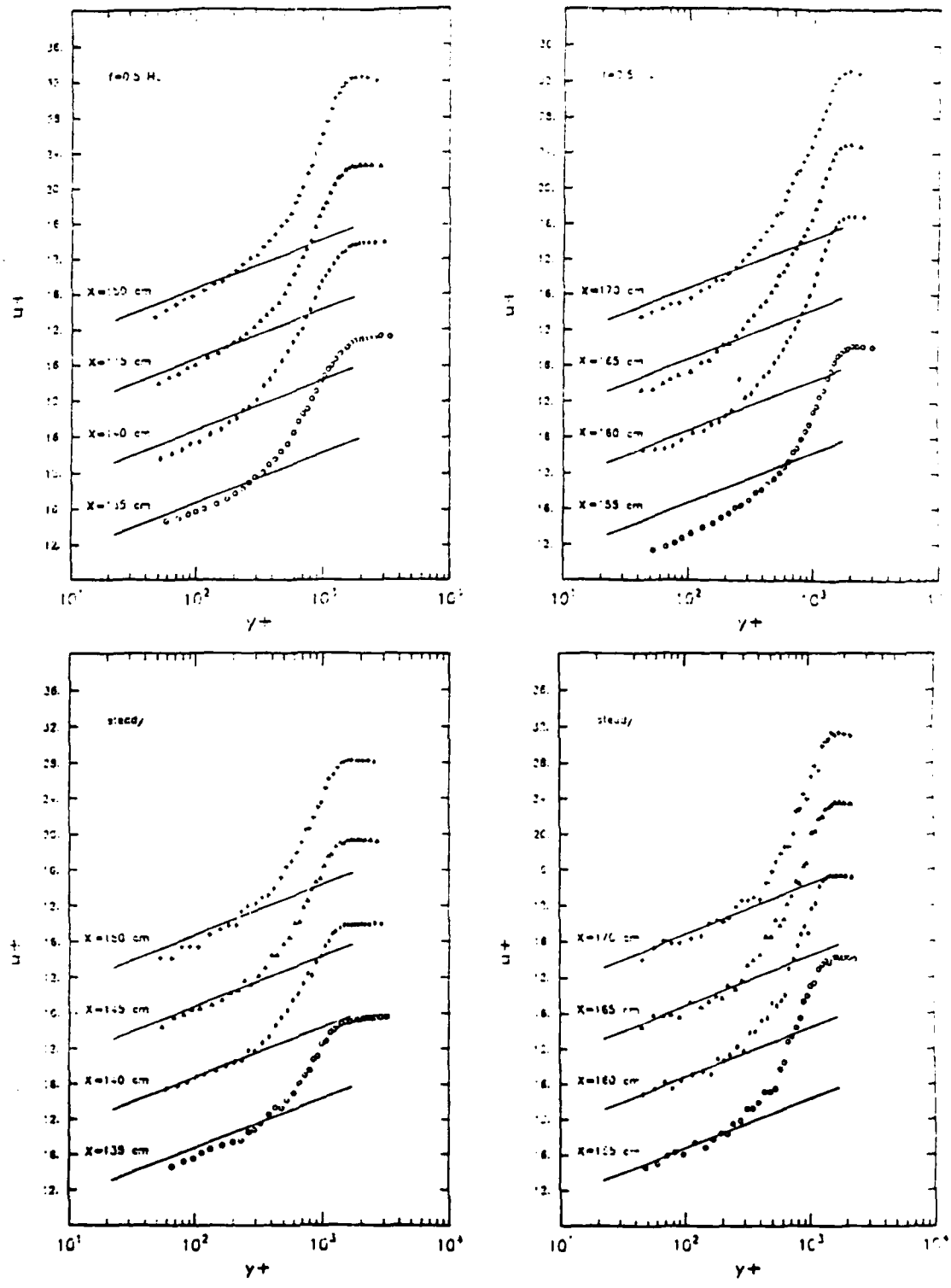

Fig.27. Time-mean velocity distributions in strong adverse pressure gradient. —, universal logarithmic law.

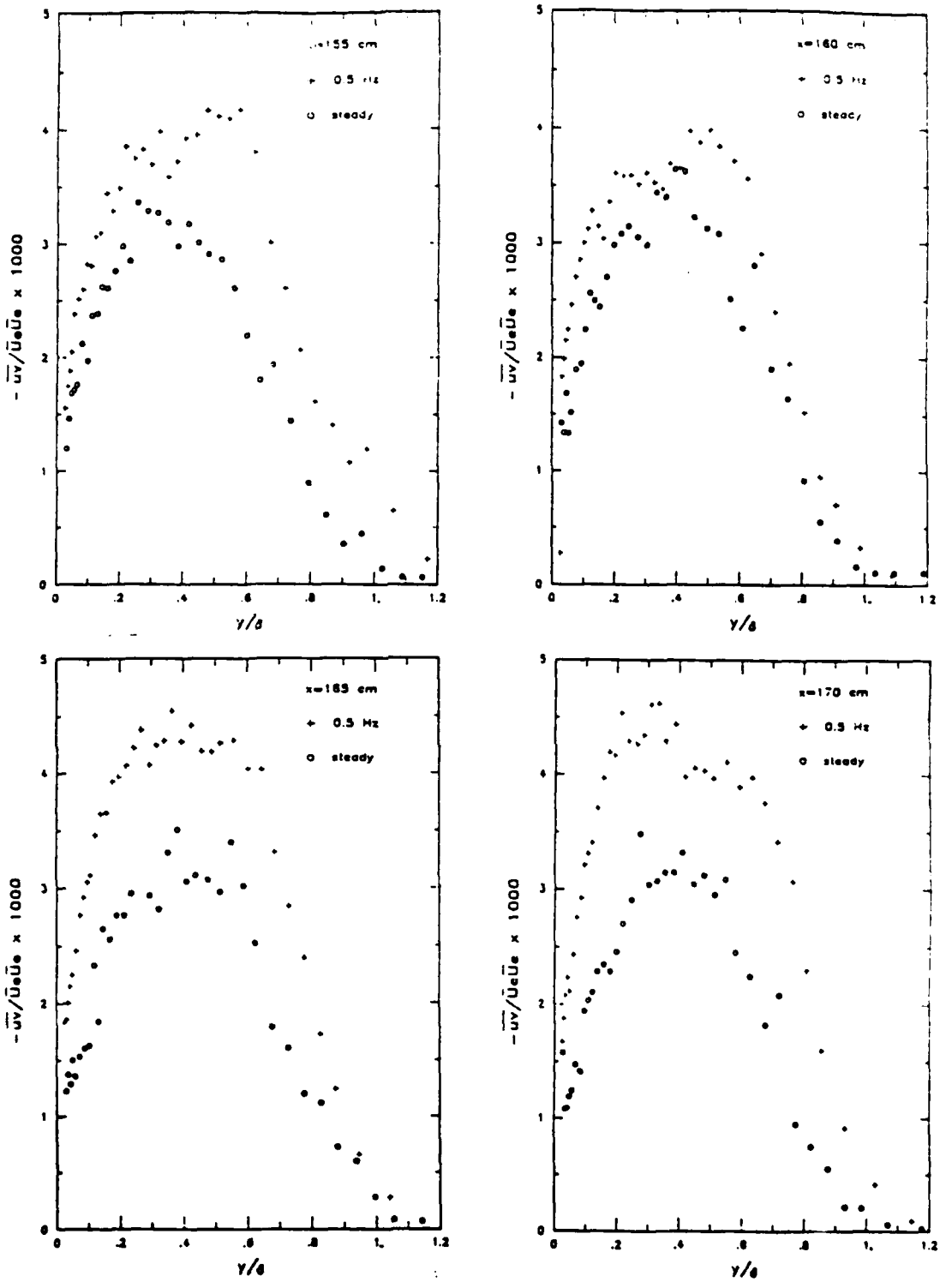

Fig.28. Long-time averaged Reynolds shear stresses in strong adverse pressure gradient.

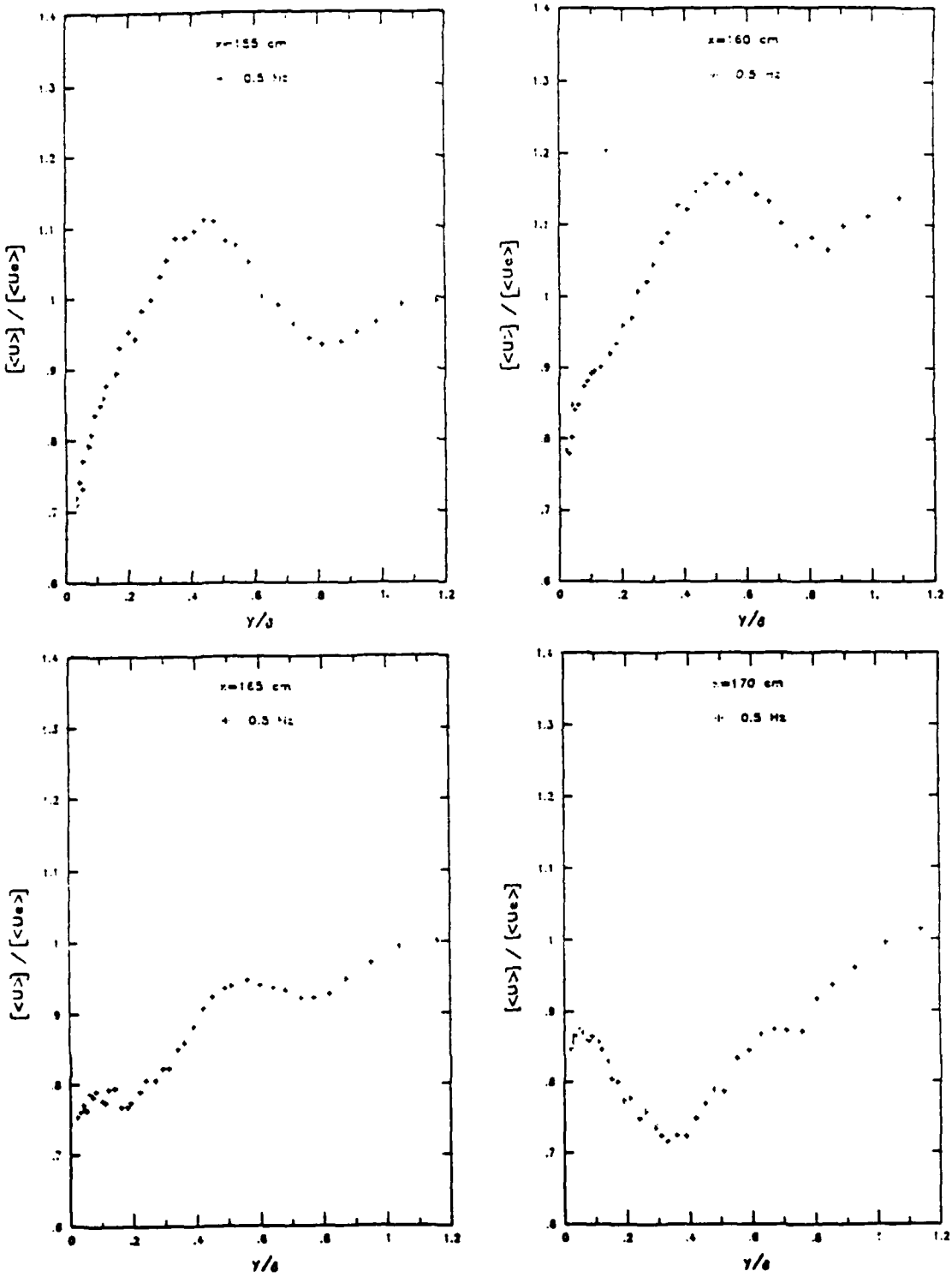

Fig.29. Distributions of the amplitude of the oscillatory velocity in strong adverse pressure gradient.

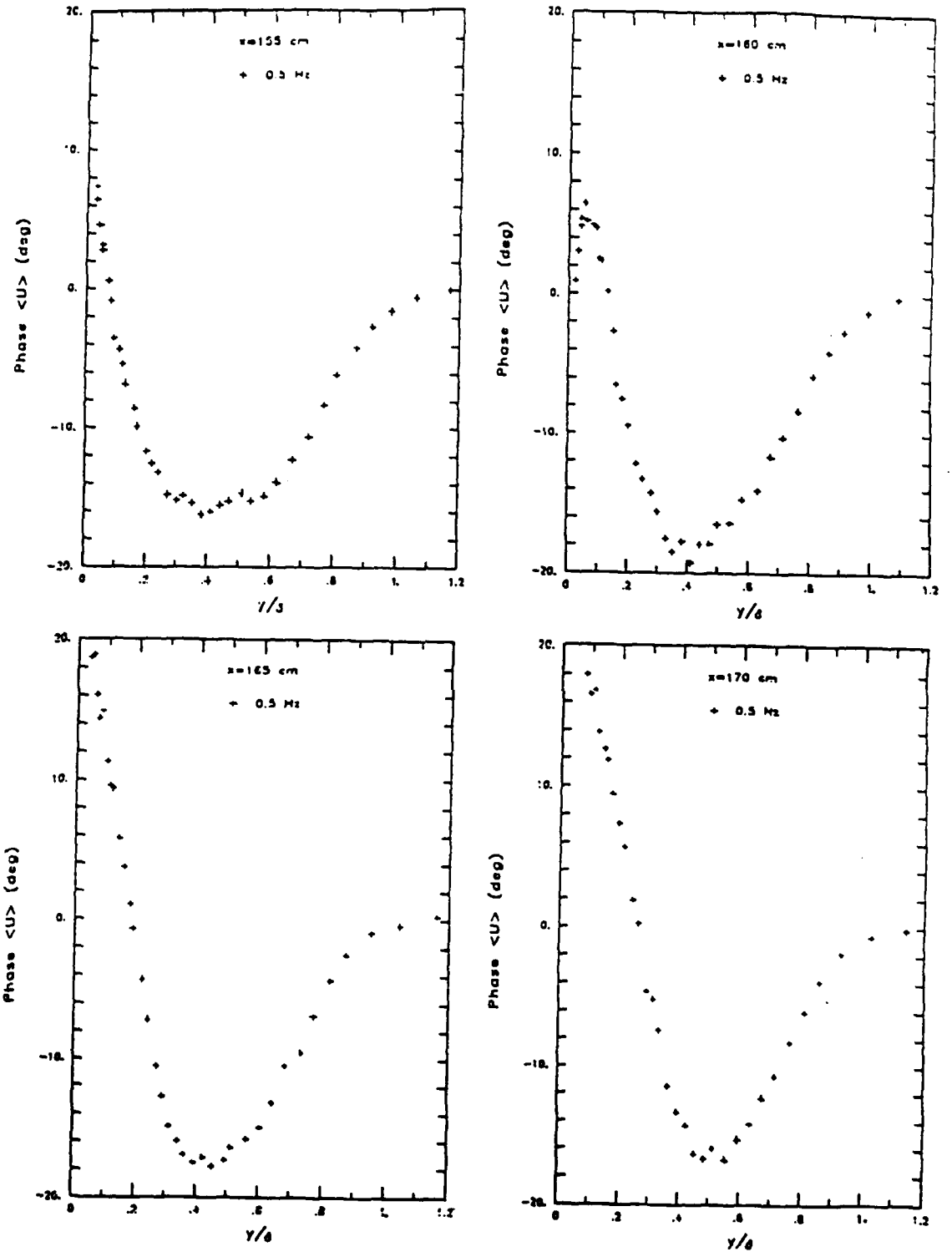

Fig.30. Distributions of the phase of the oscillatory velocity in strong adverse pressure gradient.

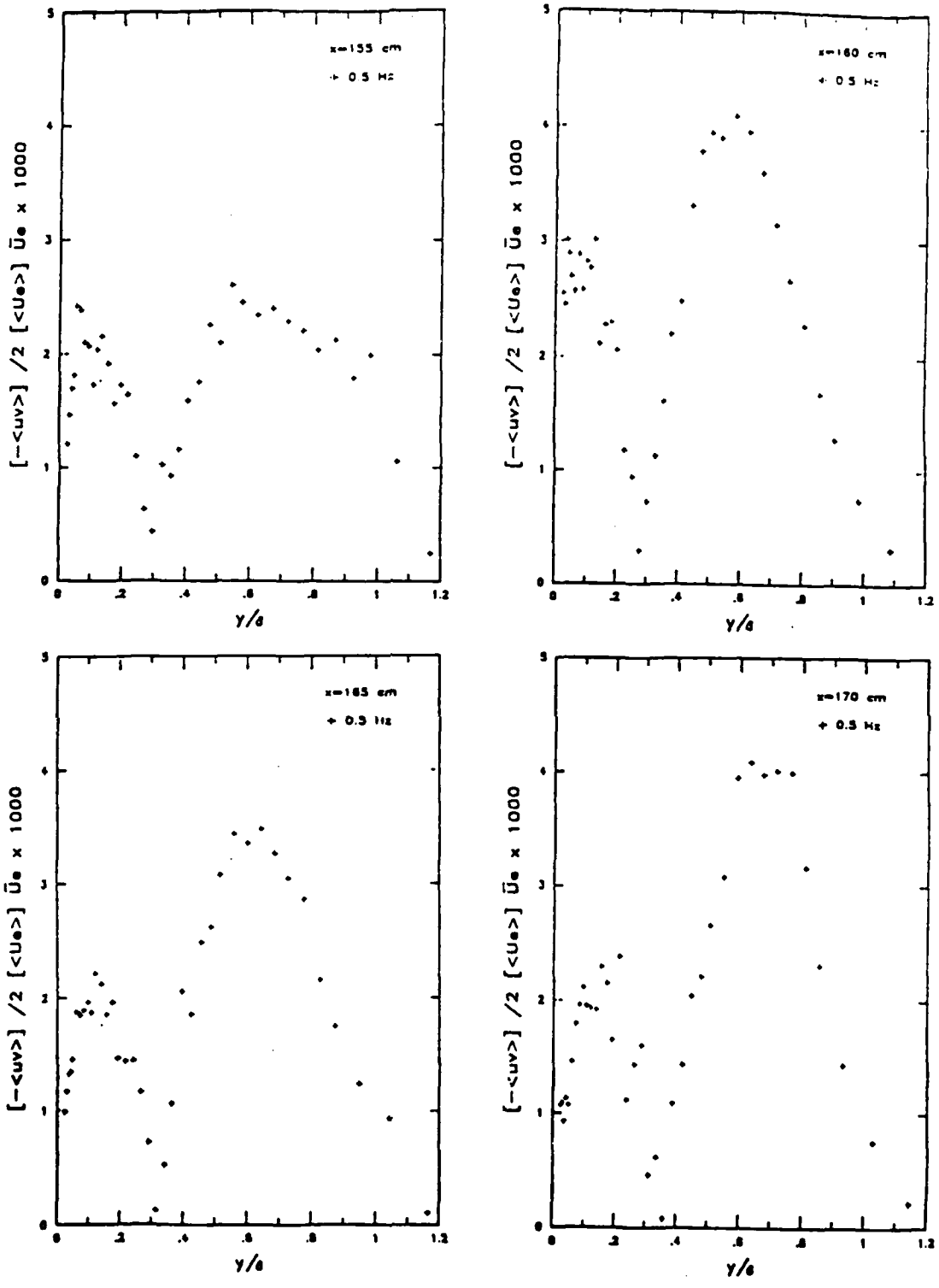

Fig.31. Distributions of the amplitude of $\langle -uv \rangle$ in strong adverse pressure gradient.

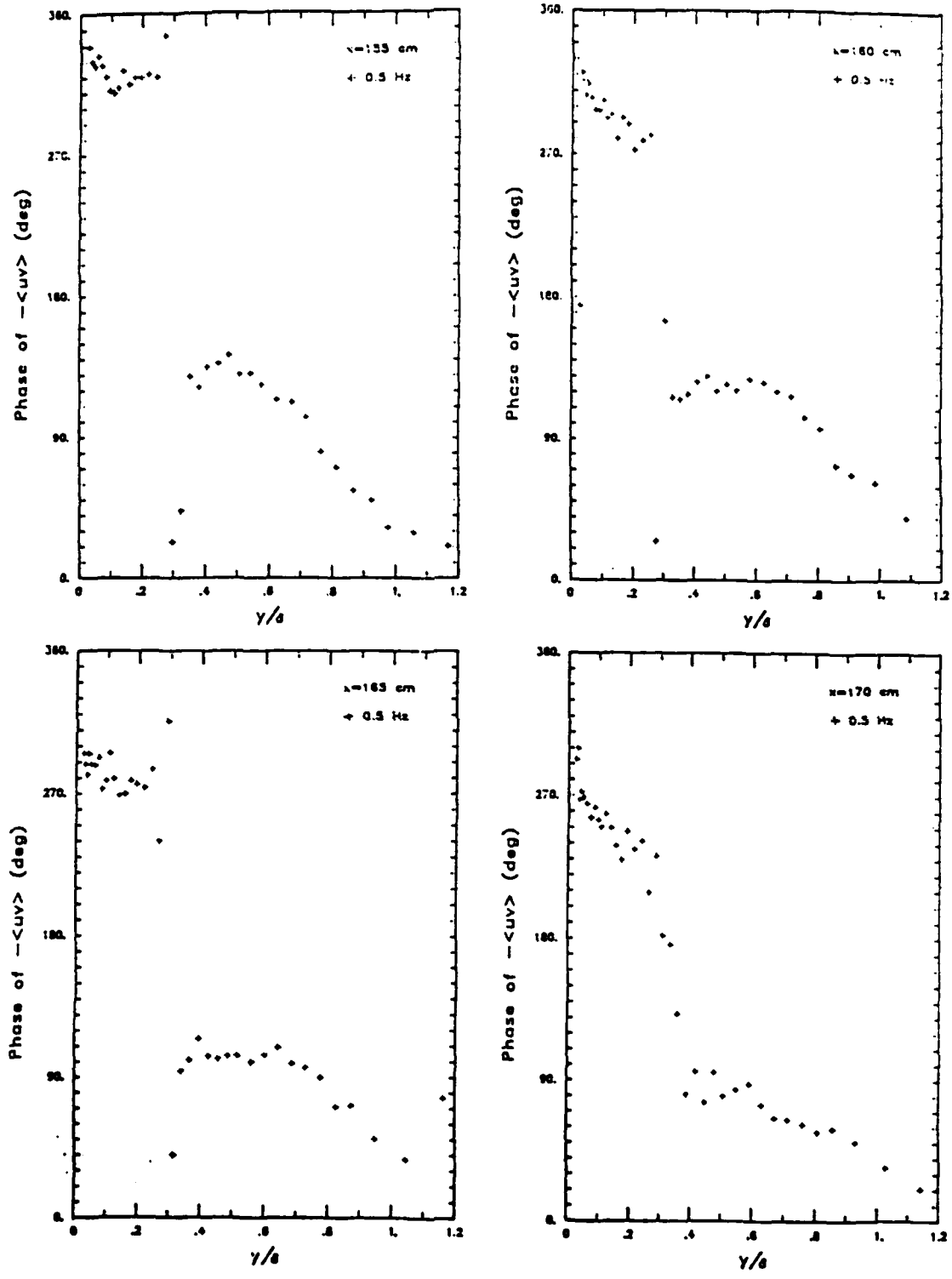

Fig.32. Distributions of the phase of $\langle -uv \rangle$ in strong adverse pressure gradient.

END

11-86

DTIC